

## Pump–Probe Polarization Anisotropy Study of Femtosecond Energy Transfer within the Photosynthetic Reaction Center of *Rhodobacter sphaeroides* R26

David M. Jonas,<sup>\*,†</sup> Matthew J. Lang, Yutaka Nagasawa, Taiha Joo,<sup>‡</sup> and Graham R. Fleming\*

Department of Chemistry and the James Franck Institute, The University of Chicago, 5735 South Ellis Avenue, Chicago, Illinois 60637

Received: March 7, 1996; In Final Form: May 6, 1996<sup>⊗</sup>

The energy transfer from the accessory bacteriochlorophylls (B) to the special pair (P) in the photosynthetic reaction center has been time resolved with pump–probe polarization anisotropy measurements using 20–25 fs duration pulses near 800 nm. The experiments were carried out at low pulse energies (500 pJ in a 34  $\mu\text{m}$  spot), low repetition rates (5 kHz), and high sample flow velocities (100 cm/s) to avoid artifacts from saturation and photoexcitation of incompletely relaxed reaction centers. The pump excitation corresponds to  $1.4 \times 10^6$  photons/ $\mu\text{m}^2$ : the “saturation intensity” for the charge separation quantum yield is  $3 \times 10^7$  photons/ $\mu\text{m}^2$ . Magic angle pump–probe transients can be satisfactorily fit as biexponential, with an  $\sim 120$  fs bleach decay followed by a 2.8 ps bleach rise. (An  $\sim 400$  fs bleach decay seen in several previous experiments arises from unrelaxed reaction centers.) The initial pump–probe anisotropy is 0.4 and decays with an  $\sim 80$  fs time constant, which we attribute to dipole reorientation by electronic energy transfer. Simultaneous kinetic modeling of the parallel, perpendicular, and magic angle pump–probe transients using the reaction center structure and dipole orientations is consistent with energy transfer proceeding in two steps:  $\sim 80$  fs electronic energy transfer from the accessory bacteriochlorophylls to the upper exciton component of the special pair ( $B \rightarrow P_+$ ) followed by an  $\sim 150$  fs internal conversion from the upper exciton component to the lower exciton component of the special pair ( $P_+ \rightarrow P_-$ ). Finally, charge separation after electron transfer from  $P_-$  to H causes an electrochromic (Stark) shift of B and produces the 2.8 ps bleach rise. The two-step energy transfer model is supported by the observation of weak quantum beat oscillations ( $125\text{ cm}^{-1}$  and  $227\text{ cm}^{-1}$ ) with near-zero anisotropy in the pump–probe signals. The near-zero anisotropy is only consistent with pump–probe signals from  $P_+$  species created by energy transfer from B. The  $\sim 80$  fs  $B \rightarrow P_+$  energy transfer is so rapid that it sets vibrational wave packets in motion on the special pair. Because  $B \rightarrow P$  energy transfer is more rapid than conventional energy transfer rates, it may be more appropriate to think of energy transfer between pigments in the reaction center as an intermediate case between energy transfer among separate pigments and internal conversion within a single supermolecule.

### I. Introduction

In photosynthesis, energy from sunlight is harvested by antennas and transferred to reaction centers.<sup>1,2</sup> At the reaction center, a rapid electron transfer initiates charge separation across a membrane. This electrochemical energy is ultimately used to drive chemical reactions. Photosynthetic energy transfer and electron transfer processes are both remarkably rapid and efficient.<sup>3</sup> The structures of the isolated reaction centers and light harvesting antennas are known for the so-called purple photosynthetic bacteria from X-ray and electron diffraction studies,<sup>4–9</sup> so that it should be possible to discern the mechanism of the fundamental energy transfer and electron transfer steps from a combination of optical spectroscopy and electronic structure theory. We report here a study of energy transfer<sup>3,10–17</sup> between chromophores in isolated reaction centers from the purple photosynthetic bacterium *Rhodobacter sphaeroides* R26 with the goal of better characterizing the interactions between pigments in the reaction center.

The reaction center contains six near-infrared absorbing pigments: a special pair of bacteriochlorophylls (P), two accessory bacteriochlorophylls ( $B_L$  and  $B_M$ ), and two bacte-

riopheophytins ( $H_L$  and  $H_M$ ). These pigments are held in a geometry with approximate  $C_2$  symmetry by the protein scaffold. Figure 1 shows two views of the special pair and accessory bacteriochlorophylls. The special pair lies on the  $C_2$  axis and is accessible from the periplasmic surface of the protein. The two bacteriochlorophylls in the special pair form a strongly coupled dimer: electronic states of the dimer are labeled with subscripts + and –, which denote symmetry or antisymmetry under exchange of the two identical chromophores. Two  $C_2$  symmetry related branches (L and M) extend toward the cytoplasmic face. Each branch contains one accessory bacteriochlorophyll and one bacteriopheophytin. Along each branch, the accessory bacteriochlorophylls are buried in the membrane and bridge the gap between P and H, making van der Waals contact with both. The spectrum of isolated reaction centers from *Rb. sphaeroides* R26 is shown in Figure 2 along with the spectra of the femtosecond laser pulses used in our study. These pulses primarily excite and probe the band near 800 nm which is composed of absorption by the two accessory bacteriochlorophyll ( $B_L$  and  $B_M$ ) and the upper exciton state of the special pair ( $P_+$ ). As shown in Figure 1, the transition dipoles between these excited states and the ground state differ significantly in direction. After excitation with a linearly polarized pump pulse, energy transfer between these states will cause changes in the average dipole orientation that can be followed by measuring the probe polarization dependence of the pump–probe signal.

<sup>†</sup> Present address: Department of Chemistry and Biochemistry, University of Colorado at Boulder, Campus Box 215, Boulder, CO 80309-0215; (303)-492-3818.

<sup>‡</sup> Present address: Department of Chemistry, Pohang University of Science and Technology, Pohang, 790-784 South Korea.

<sup>⊗</sup> Abstract published in *Advance ACS Abstracts*, July 1, 1996.

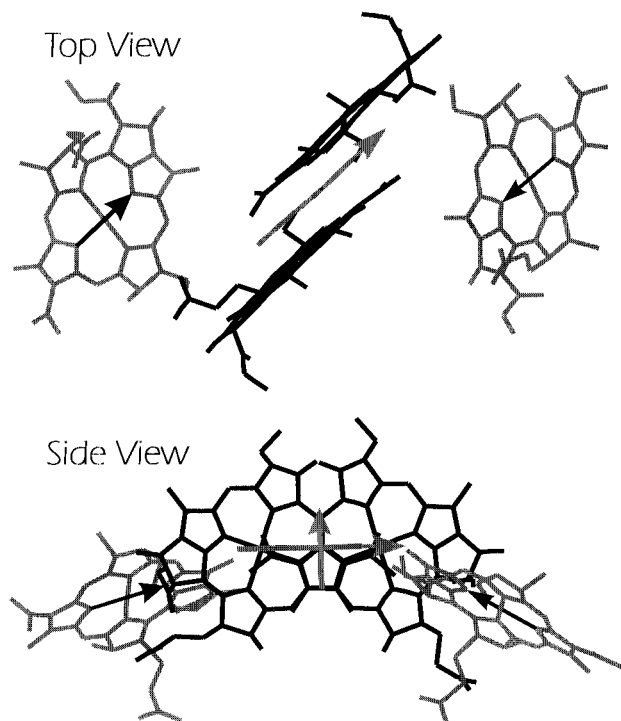


**Figure 1.** (Top) View of special pair and accessory bacteriochlorophylls in the reaction center of *Rb. sphaeroides* looking down from the periplasmic face along the transition dipole for the upper exciton state ( $P_+$ ) of the special pair (pointing out of the plane of the figure and not shown). Coordinates for the special pair and accessory bacteriochlorophylls without their phytol chains are taken from Chang et al.<sup>6</sup> The L branch accessory bacteriochlorophyll is on the right, the M branch accessory bacteriochlorophyll is on the left, and the special pair of bacteriochlorophylls are in the middle. Arrows show the projection of the  $Q_y$  transition dipoles onto the plane of the figure for both accessory bacteriochlorophylls and the lower (antisymmetric) exciton state of the special pair  $P_-$  (points left to right and up). In this projection, all three transition dipole moments appear to be nearly parallel. (Bottom) Side view of reaction center from *Rb. sphaeroides* showing special pair and accessory bacteriochlorophylls. The L side accessory bacteriochlorophyll is on the right, the M side accessory bacteriochlorophyll is on the left, and the special pair bacteriochlorophylls are in the middle. The periplasmic face of the protein lies above the pigments, and the cytoplasmic face is below. Arrows show the projection of the  $Q_y$  dipoles onto the plane of the figure for both accessory bacteriochlorophylls and both exciton states of the special pair  $P_+$  (points up) and  $P_-$  (points left to right).

A number of theoretical calculations have addressed the couplings between the hexamer of pigments in the reaction center<sup>18–25</sup> with the goal of interpreting both spectroscopic properties (absorption spectra, linear dichroism, resonance Raman, photochemical hole burning) and electron transfer dynamics. These studies generally find some degree of coupling between all pigments in the hexamer. The two bacteriochlorophylls of the special pair have extensively delocalized excitations that are close to symmetric and antisymmetric combinations of monomeric excitations. The antisymmetric state  $P_-$  is reached by a strong band at 870 nm. At room temperature, the transition to the symmetric state  $P_+$  overlaps the accessory bacteriochlorophyll bands at 800 nm, but it appears as a shoulder near 810 nm at low temperature.<sup>18,21–23,26</sup> The two accessory bacteriochlorophylls absorb light at 800 nm. Some calculations indicate that the accessory bacteriochlorophylls may act as a dimer because of indirect coupling through mutual interactions with the special pair.<sup>21–24</sup> Calculations agree that the bacterioopheophytins, which absorb near 755 nm, function as monomers, and spectroscopic transitions to  $H_L$  and  $H_M$  can be resolved at low temperature. More recent theoretical work has focused mainly on the states involved in the primary electron

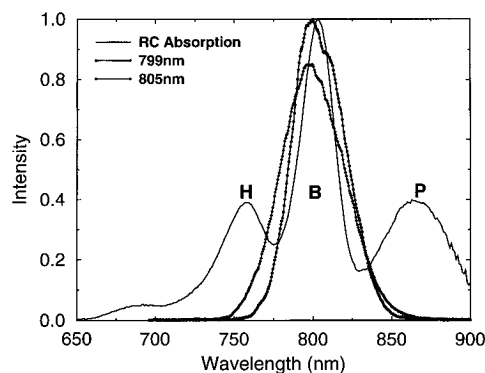


**Figure 2.** Absorption spectrum (solid line) of reaction centers from *Rb. sphaeroides* R26 suspended in LDAO recorded at 293 K. The bands are labeled P (transition to the lower exciton state of the special pair), B (accessory bacteriochlorophylls), and H (bacterioopheophytins) according to the dominant absorbing species in that region. A transition to the upper exciton state of the special near 810 nm accounts for roughly one-quarter of the intensity of the 800 nm peak labeled B. The spectrum of the excitation pulses is also shown: (diamonds) 799 nm center wavelength, 49 nm bandwidth pulses of 20.2 fs duration; (circles) 805 nm center wavelength, 40 nm bandwidth pulses of 25.5 fs duration.

transfer, which proceeds from  $P_-$  to  $H_L$ .<sup>27–33</sup> In simulating the optical spectra, the interactions between pigments in the reaction center have usually been approximated as excitonic transition–dipole coupling<sup>21–24</sup> although some studies<sup>18,19</sup> have included the transition dipole charge distribution.<sup>34</sup> Since the same coupling terms between pigments are responsible for both excitonic coupling and energy transfer,<sup>10,11</sup> these calculations suggest that energy transfer from the accessory bacteriochlorophylls to the special pair lies in the strong coupling (coherent) limit<sup>10</sup> and that weak coupling (hopping) calculations of the energy transfer rate are inadequate.<sup>26</sup>

Several experiments have shown that excitation of a band assigned to one pigment produces bleaching of bands assigned to other pigments in less than 100 fs.<sup>35,36</sup> With 100 fs time resolution, Breton et al.<sup>35</sup> have reported an instrument limited rise of  $P_-$  bleaching upon excitation of B or H and estimated that the energy transfer from  $B^*$  to P is faster than 100 fs. In principle, an unresolved bleach rise can indicate either strong excitonic coupling between pigments or an unresolved energy transfer event: the two can be distinguished by observation of a nonzero bleach rise time or transitions which originate in the excited state of the acceptor. Both of these studies also reported a 400 fs bleach decay component which accompanies B to P energy transfer. More recent work indicates that the special pair is electronically excited within 100 fs after excitation of B. A report<sup>37</sup> that an 800 nm pump pulse yielded an instrument limited rise time for mid-infrared  $P^*$  absorption suggests that energy is transferred from B to  $P^*$  in less than 100 fs, and a more recent study with 100 fs pulses obtained a 120 fs time constant for energy transfer from B to  $P_-$ .<sup>38</sup> After this paper was submitted, Haran et al. published pump–probe polarization anisotropy measurements in which reaction centers were excited with 100 nJ pulses of 40–60 fs duration centered at 810 nm and probed with 60 fs pulses centered at 950, 1200, and 3840 nm.<sup>39</sup> In our laboratory, Bradforth, Dikshit, and Jimenez<sup>40</sup> excited B using 90 fs pulses with an 11 nm bandwidth centered at 797 nm and detected  $P_-$  fluorescence polarized perpendicular to the excitation pulse over a  $\sim 10$  nm band pass around 930 nm by fluorescence up-conversion and found that a rise time of  $\sim 120$  fs was required to fit an asymmetry between the lower and upper portions of the initial rise. This result is consistent with the statement of Stanley and Boxer<sup>41</sup> that a rise time was required to fit  $P_-$  emission at 955 nm following excitation at 803 nm. Upon excitation of B, a charge transfer quantum yield

of 0.93 has been reported.<sup>42</sup> Recently, Hartwich et al. reported a charge transfer quantum yield of 1 upon  $P_+$  excitation.<sup>43</sup> Michel-Beyerle and co-workers<sup>44</sup> have also reported a fluorescence up-conversion study of  $B^* \rightarrow P_-$  energy transfer. The  $P_-$  fluorescence rise time does not directly measure the energy transfer rate: the analysis of depolarization data presented here indicates that energy is transferred from B to  $P_+$  and that  $P_+$  undergoes internal conversion to  $P_-$ .

In a preliminary communication,<sup>45</sup> we presented pump-probe transients obtained at 152 kHz repetition rate with pulses centered at 805 nm for which the pump and probe polarizations were parallel. In the preliminary experiments, we observed a biexponential decay with time constants of 120 and 400 fs for both normal reaction centers and reaction centers in which the special pair had been chemically oxidized with potassium ferricyanide.<sup>40</sup> Further investigation has revealed two defects in our prior data: each sample volume was excited by many ( $\sim 20$ –80) laser pulses so that the pump-probe signal was not zero when the probe arrived at the sample before the pump; the 1.5 nJ pulse energy saturated the reaction centers and distorted the temporal shape of the pump-probe transient. The experiments reported here were carried out at lower pulse energies (500 pJ), high sample flow velocities (100 cm/s), and a 5 kHz repetition rate in order to avoid saturation and multiple excitations. For normal reaction centers, pump-probe transients recorded under these conditions exhibit both a faster initial bleach decay (with no 400 fs component) and a larger charge separation quantum yield than data obtained at higher repetition rates or higher pulse energies.<sup>40,45</sup>

## II. Experimental Section

The pump-probe depolarization experiment required short pulses of light with controlled polarization, low pulse energies (pump, 500 pJ/pulse; probe, 70 pJ/pulse), low repetition rates (5 kHz), small spot size ( $34 \mu\text{m}$  1/e), and high sample flow rates (100 cm/s) to avoid problems associated with scattering, saturation, and excitation of unrelaxed reaction centers. The photon flux must be kept low to avoid exciting more than one accessory bacteriochlorophyll within a single reaction center. The flow rate is limited by the tendency of the detergent to foam at high speeds. Most of the noise in our experiment comes from relatively rare events in which the pump (or probe) scatters off a single particle or bubble in the sample, which makes it impractical to lower the repetition rate and increase both spot size and pulse energy to avoid saturation. These constraints are interlinked and necessitated careful optical layout, electronic timing, and signal recovery.

**A. Materials.** Reaction centers of *Rb. sphaeroides* R26 which had been isolated, purified, and suspended in BOG and LDAO detergents<sup>46</sup> were generously supplied by Julia Popov, S. N. Dikshit, and James R. Norris. The samples were concentrated by centrifuging and filtered with  $0.22 \mu\text{m}$  filters to remove scattering particles. At 800 nm, the optical densities of the BOG and LDAO samples were 0.07 and 0.1, respectively, in a  $200 \mu\text{m}$  path. The total volume of  $\sim 3$  mL was chilled in ice water and stored in the dark throughout pump-probe depolarization measurements. During data collection the signal was monitored for scattering and retention of the 2.8 ps bleach rise due to electron transfer, and absorption spectra were taken to monitor sample degradation. We found that the 2.8 ps rise was more sensitive to sample degradation than the absorption spectrum. After every 6 h of data collection, it was necessary to remove, centrifuge, and filter the sample to remove scattering particles and bubbles. Data collection typically required a total of 24 h. Measurements on normal reaction centers were followed by ones in which the special pair had been chemically oxidized by potassium ferricyanide.<sup>40</sup>

**B. Laser System.** The Kerr lens mode-locked Ti:sapphire laser was home-built according to the design of Asaki et al.<sup>47</sup> The laser was pumped with 5.2 W all lines from a Coherent Innova 310 Argon ion laser and cavity dumped with an acousto-optic Bragg cell to lower the repetition rate to 5 kHz.<sup>48</sup> The pulse energy was most stable (fluctuations  $< 0.7\%$  peak to peak) when cavity dumping efficiency was maximized to dump  $\sim 40$  nJ/pulse: most of this energy was not used. Care was taken to avoid an  $N = 2$  soliton mode of the cavity which produced two pulses per cavity round trip at unequal time intervals. The spectrum of the laser was tuned to match the 800 nm absorption maximum<sup>2</sup> of B by translating the oscillator intracavity prism, yielding pulses of  $\sim 20$ –25 fs duration. A double pass through a pair of LaKL21 prisms precompensated for material dispersion of the subsequent optics. The spectrum was shaped to nearly Gaussian by means of razor blades at the external pulse compression prism pair to yield a center wavelength of 799 nm (805 nm) with a 49 nm (40 nm) bandwidth. Experiments were run at these wavelengths to monitor both sides of the B band (see Figure 2). The dispersion of the pump and probe beam paths were matched with identical optics. The pump and probe pulses were cross correlated with non-collinear type I second harmonic generation in a  $100 \mu\text{m}$  thick  $\beta$ -BBO crystal at the sample position (Figure 3). Fits to a Gaussian envelope yielded pulse durations of 20.2 fs (25.5 fs). The resulting time bandwidth product was 0.455 (0.466), close to the Gaussian transform limit of 0.441. Short pulses were needed to resolve the fast dynamics of the experiment.

**C. Optical Layout.** The optical arrangement of the pump-probe experiment is shown in Figure 3. After prism compression, the beam passed through an 800 nm zero-order  $\lambda/2$  wave plate used to set the probe power and was split into pump, probe, and reference beams. The pump beam traveled through a chopper, an 800 nm zero-order  $\lambda/2$  wave plate, a fixed delay, and a polarizer and was reflected off a mirror so that it was parallel to the probe beam. The probe beam was sent along a computer-controlled delay stage and passed through a polarizer and an 800 nm zero-order  $\lambda/2$  wave plate. The pump and probe paths had matched wave plates and polarizers. The reference beam traveled through a variable silver coated neutral density wheel and was directed onto a photodiode.

Care was taken to get the cleanest possible polarization at the sample. The pump polarizer was set for vertical polarization and this was preserved by one "s" reflection off a mirror between it and the sample. The probe beam was set for vertical polarization by a polarizer, and this polarization was rotated by an 800 nm zero-order  $\lambda/2$  wave plate immediately prior to the sample. The parallel pump and probe beams were separated by 8 mm and focused into the sample by a 10 cm focal length fused silica lens. The pump and probe beams were overlapped at the focus by maximizing their transmission through a  $30 \mu\text{m}$  pinhole. The extinction and transmission of the polarizations were tested with a polarizer placed at the sample. Extinction was at least 5000:1 for all pump and probe polarizations. The probe wave plate angle could reproducibly be set to within a precision of 1 min. By measuring probe transmission through a  $50 \mu\text{m}$  pinhole at the sample, it was determined that the pump-probe overlap at the sample was unaffected by probe wave plate rotation and delay stage translation to within 1%. The width of the pump-probe cross correlation was unaffected by probe polarization rotation to within our measurement precision (0.1 fs). The pump-probe depolarization experiment was also tested by measuring the anisotropy of HITCI and IR144 dyes in methanol at 125 pJ power levels: it was experimentally verified that the pump-probe anisotropy was less than 0.01 at 1 ns pump-probe delay; the initial anisotropy was found to be

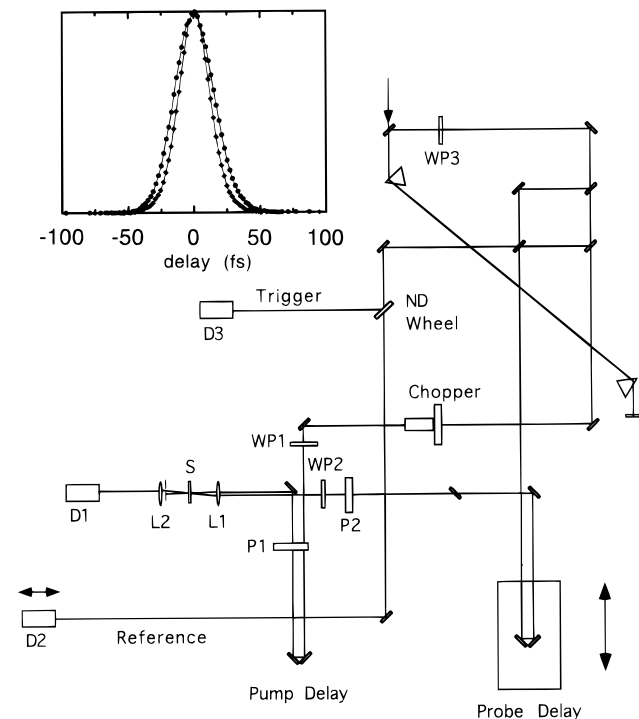


**Figure 3.** Pump-probe experimental configuration. Arrow shows cavity dumped beam from Ti:sapphire oscillator. WP: zero-order half wave plates for pump power (WP1), probe polarization (WP2), and probe power (WP3) adjustments; P: matched glan-laser polarizers for pump (P1) and probe (P2) both oriented for vertical polarization; L: 10 cm focusing (L1) and collimating (L2) lenses; D: photodiodes for detecting the probe (D1) and reference (D2) beams and triggering the boxcar (D3). After passing through polarizer P1, the vertically polarized pump beam is directed into the sample by one "s" reflection off a mirror. After the probe beam passes through polarizer P2, the polarization is adjusted with the half wave plate WP2 and passes directly through the sample and onto the probe photodiode D1 without any mirror reflections. The half wave plate WP3 is used to set the probe power by adjusting the transmission through polarizer P2. The pump power is independently adjustable using the half wave plate WP1 to adjust transmission through polarizer P1. The pump and probe beams cross at an angle of  $5^\circ$  in the  $200\ \mu\text{m}$  pathlength sample cell (S). Note that the pump and probe beams travel through matched optics on their path to the sample. An iris diaphragm blocks the pump beam between the sample (S) and the collimating lens (L2). D1 and D2 are matched photodiodes which are positioned for identical optical path lengths of the probe and reference beams. The outputs of D1 (probe) and D2 (reference) are fed into a fast differential amplifier which is nulled in the absence of the pump by adjusting the variable neutral density filter (ND Wheel). The output of the differential amplifier is fed into a boxcar triggered off photodiode D3. The boxcar output is fed into a lock-in amplifier referenced to the pump chopping frequency which detects the pump-induced change in the probe intensity transmitted through the sample as a function of pump-probe delay. (Inset) Non-collinear pump-probe cross-correlations recorded at the sample position by type I second-harmonic generation in a  $100\ \mu\text{m}$  thick  $\beta$ -BBO crystal. Spot size was  $34\ \mu\text{m}$  and crossing angle was  $5^\circ$ : (diamonds)  $799\ \text{nm}$  [(circles)  $805\ \text{nm}$ ], center wavelength;  $49\ \text{nm}$  ( $40\ \text{nm}$ ), spectral full width at half-maximum; Gaussian fits yielded a pulse duration of  $20.2\ \text{fs}$  ( $25.5\ \text{fs}$ ). The resulting time bandwidth product was  $0.455$  ( $0.466$ ).

$0.392$  for HITCI and  $0.3992(\pm 6)$  for IR144. Our measured anisotropy decay for  $1.2\ \text{mM}$  HITCI in methanol is slightly faster,  $\tau = 179(18)\ \text{ps}$ , than that reported previously.<sup>49</sup> Accurate anisotropy measurements require low pulse energy to avoid saturation artifacts (see below). Figure 4 shows an experimental reaction center magic angle pump-probe signal and a magic angle signal calculated directly from the experimental parallel and perpendicular signals using the relationship  $I_{\text{MA}}(t) = (1/3)(I_{\text{PA}}(t) + 2I_{\text{PE}}(t))$ . No adjustable parameters were used in this comparison, which shows the quality of the polarization used in the experiment.

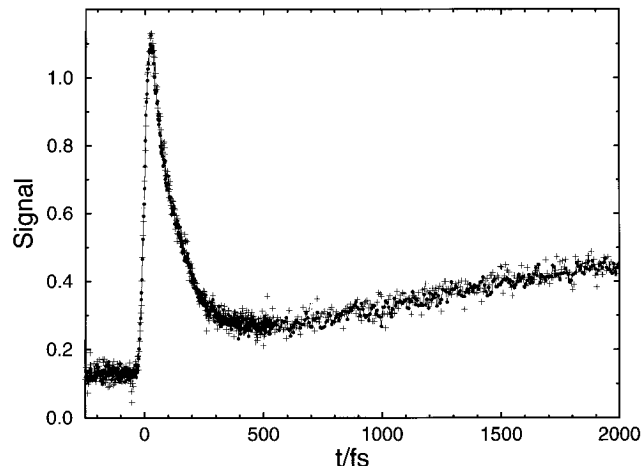


**Figure 4.** Transient absorption of *Rb. sphaeroides* R26 reaction centers recorded with  $25.5\ \text{fs}$  pump and probe pulses of  $40\ \text{nm}$  bandwidth (fwhm) centered at  $805\ \text{nm}$ . Crosses (+) denote experimental pump-probe data recorded with the probe polarization at the magic angle to the pump polarization. Dots ( $\bullet\bullet\bullet$ ) mark a magic angle pump-probe transient calculated from the parallel and perpendicular transients without any adjustable parameters using the relation  $I_{\text{MA}} = (1/3)(I_{\text{PA}} + 2I_{\text{PE}})$ . The constructed signal overlaps the magic angle signal showing the agreement between experimental data sets obtained with different pump-probe polarizations. Experimental conditions:  $500\ \text{pJ}$  pump pulse energy,  $70\ \text{pJ}$  probe pulse energy,  $34\ \mu\text{m}$  beam diameter,  $5\ \text{kHz}$  repetition rate,  $\sim 100\ \text{cm/s}$  sample flow rate.

Powers were set by changing the polarization of the initial beam with a wave plate to set the probe power and rectifying the polarization with a wave plate along the pump beam path to set the pump power. The reference power was set to match the probe by rotating the variable neutral density wheel. A fast ( $2\ \text{ns}$  rise time) red-sensitive photodiode collected the probe beam directly after it passed through the sample (mirror reflections were not used because they are polarization dependent).

**D. Timing System.** Stable cavity dumping at  $5\ \text{kHz}$  required a divided signal referenced to the repetition rate of the laser. The oscillator round trip frequency was monitored with a photodiode behind the high reflector. Because up to  $90\%$  of the intracavity pulse energy was dumped out of the oscillator cavity, the photodiode output was sent into a constant-fraction discriminator to produce a uniform  $76\ \text{MHz}$  signal. The  $76\ \text{MHz}$  frequency signal was divided down to  $38\ \text{MHz}$  and amplified. Two master clocks and an RF pulse generator were phase locked to the  $38\ \text{MHz}$  signal. One master clock (Camac TS 2000) generated a  $5\ \text{kHz}$  signal to trigger the RF pulse generator (Camac CD 1000) used for cavity dumping at  $5\ \text{kHz}$ . A second master clock (Camac TS 2000) was used to set the  $500\ \text{Hz}$  chopper frequency and phase.

**E. Signal Detection.** The  $5\ \text{kHz}$  repetition rate necessitated by the maximum flow rate yields a duty cycle of about  $10^{-5}$  (signal of a few nanoseconds duration every  $200\ \mu\text{s}$ ). This low duty cycle greatly reduces the efficiency of lock-in detection, but the signal level was too low for simple gated integration. A hybrid technique was used in which a gated integrator increased the duty cycle of the lock-in signal input. The probe and reference beams were detected by matched photodiodes. The reference power and delay were adjusted to match the probe in the absence of the pump. The probe and reference signals were differentially amplified by a high-speed wide-band transconductance amplifier (MAXIM #436). The output of the differential amplifier was amplified  $10\times$  by a LeCroy (LRS 234) amplifier and sent into a gated integrator and boxcar (SR250). For maximum accuracy in gate position, the boxcar was triggered with a photodiode. The boxcar integrated the dif-

ferential amplifier output for each pulse over a 10 ns gate and sent a voltage proportional to the differential amplifier output on the last pulse to the lock-in (ORTEC 9503).

The lock-in was referenced to the 500 Hz frequency pump beam chopper. Because the chopper frequency of 500 Hz is one-tenth the 5 kHz pulse repetition rate, the chopper was synchronized to the cavity dumper so that five pulses passed the chopper and the next five were blocked. A wide-slot six-blade chopper was used to avoid beam clipping. (An unsynchronized or clipping chopper will drift and allow more or less than five pulses through, obscuring the signal.) The lock-in time constant was set to 10 ms to allow fast recovery from laser scattering off bubbles and particles. The output of the lock-in was fed to an A/D converter (SR245).

**F. Measurements.** Measurements on the reaction centers in BOG were carried out with 20.2 fs pulses centered at 799 nm, while measurements on reaction centers in LDAO were carried out with 25.5 fs pulses centered at 805 nm. The pump and probe powers were set to 500 and 70 pJ, respectively (see below). Immediately prior to depolarization measurements on the reaction centers, we checked that the initial anisotropy of IR144 matched the expected (slightly saturated) value of 0.38 for 500 pJ pump energy. The reaction center flow cell and peristaltic pump were then substituted for the dye cell. The flow velocity was increased while monitoring the pump–probe signal at  $-1$  ps delay until the nonzero baseline due to reaction centers remaining in the sample volume from the previous pulse was eliminated. The measured flow velocity was 1.4 mL/s. Assuming uniform flow, this corresponds to a linear velocity of 90 cm/s in the  $200 \mu\text{m} \times 8$  mm rectangular cell. Laminar flow calculations<sup>50</sup> which approximate the rectangular cross section as an ellipse of the same area yield an average velocity of 120 cm/s through the focus of the laser beams. The slowest 10% of reaction centers have an average linear velocity of 17 cm/s, sufficient for the sample to completely flow through a  $34 \mu\text{m}$  diameter spot between laser shots at 5 kHz repetition rate.

**G. Saturation.** The laser beam spot size in the sample was determined by measuring the transmission through two pinholes. The transmission was 85% for a  $50 \mu\text{m}$  diameter pinhole and 64% for a  $30 \mu\text{m}$  diameter pinhole. Modeling the focal spot as Gaussian,  $I(r, \theta) = (1/(\pi w^2)) \exp(-r^2/w^2)$ , we calculate a  $1/e$  diameter of roughly  $34 \mu\text{m}$  ( $w = 17 \mu\text{m}$ ).

Using a power meter, it was determined that 10% of the incident 500 pJ pulse energy was absorbed in the  $200 \mu\text{m}$  path through the LDAO sample, which corresponds to absorption of  $2 \times 10^8$  photons. From the  $5/\text{cm}$  optical density of the sample at 800 nm and the  $3 \times 10^5/\text{M}\cdot\text{cm}$  extinction coefficient of reaction centers at 800 nm,<sup>2</sup> we calculate a reaction center concentration of  $1.66 \times 10^{-5}$  M. The  $1/e$  volume ( $V = (200 \mu\text{m})\pi(17 \mu\text{m})^2 = 1.82 \times 10^{-10}$  L) contains  $1.82 \times 10^9$  reaction centers which absorb  $1.26 \times 10^8$  photons: 7% of the reaction centers are excited by the pump pulse. If the excitation probabilities for the two accessory bacteriochlorophylls are independent, 7% of the excited reaction centers will be doubly excited. (Strictly speaking, the excitation probabilities are not independent because of the  $\sim 45^\circ$  angle between transition moments on  $B_L$  and  $B_M$ , so less than 7% of the reaction centers should be doubly excited.) A doubly excited reaction center can produce only one charge transfer event even though it has absorbed two photons.

Pump–probe transients at higher pump intensities are saturated and have a distorted bleach decay (Figure 5). Our rationale for measuring saturation at 4 ps delay was that charge separation should occur after energy transfer in reaction centers which function normally. The saturation of reaction center charge transfer was determined by monitoring the pump–probe signal

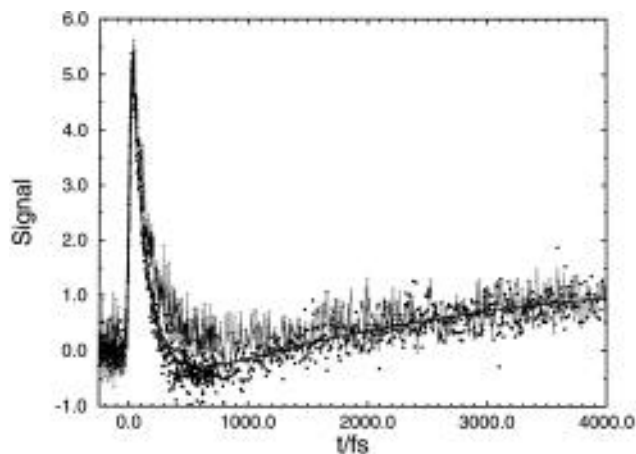


**Figure 5.** Transient absorption of *Rb. sphaeroides* R26 reaction centers recorded with 20.2 fs pump and probe pulses of 49 nm bandwidth (fwhm) centered at 799 nm. The signal was recorded with the probe polarization at the magic angle to the pump polarization. The pulse energies were 500 pJ (dots) and 4 nJ (crosses), the Gaussian  $1/e$  spot size was  $34 \mu\text{m}$  in diameter, the repetition rate was 5 kHz, and the flow rate was  $\sim 100$  cm/s, which is sufficiently rapid to ensure that each sample volume was refreshed between pump pulses. The pump–probe signal at 4 nJ pump pulse energy has been divided by a factor of 5.1 to match the initial amplitude of the 500 pJ signal. In the absence of saturation, the 4 nJ signal would match the amplitude of the 500 pJ signal when divided by 8 rather than 5.1. Note the faster early dynamics in the 500 pJ signal.

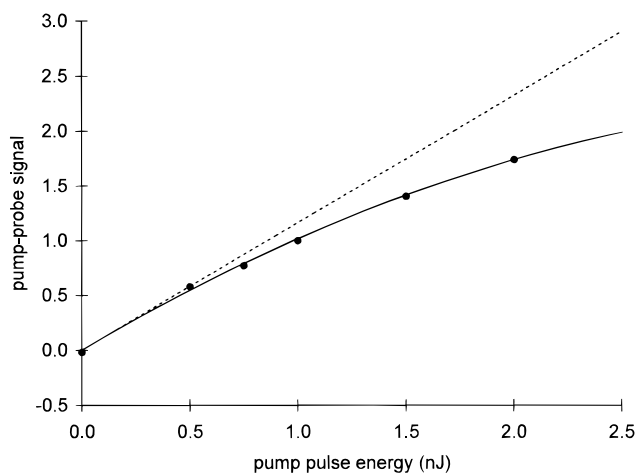


**Figure 6.** Pump–probe signal at 4 ps delay as a function of the pump pulse energy. Pump and probe pulses were centered at 805 nm and had durations of 25.5 fs, Gaussian  $1/e$  beam diameters of  $34 \mu\text{m}$ , and parallel polarizations. The probe pulse energy was 50 pJ for all measurements. Experimental points (dots) were corrected for pump and probe scattering by subtracting the pump–probe signal at  $-1$  ps delay from the pump–probe signal at 4 ps delay. The solid line is a linear least squares fit to the equation:  $S = aI - bI^2$ , where  $S$  is the pump–probe signal,  $I$  is the pump pulse energy, and  $a$  and  $b$  are fit parameters. The linear component of the signal is shown as a dashed line. The saturation pulse energy given by the ratio  $I_s = (a/b)$  is 8 nJ ( $8 \text{ pJ}/\mu\text{m}^2$  or  $3 \times 10^7$  photons/ $\mu\text{m}^2$ ). At the saturation intensity, the charge transfer quantum yield would be reduced by a factor of 2 relative to the low-intensity limit if no additional nonlinear processes appear below the saturation intensity. A saturation of 6% was determined under the experimental conditions of 500 pJ/pulse. The saturation intensity of  $3 \times 10^7$  photons/ $\mu\text{m}^2$  agrees reasonably well with a decrease in the charge separation quantum yield observed by Breton et al. above  $2 \times 10^7$  photons/ $\mu\text{m}^2$  for excitation of the accessory bacteriochlorophylls in isolated reaction centers from *Rps. viridis*.<sup>35</sup>

at 4 ps delay as a function of pump pulse energy (see Figure 6). The signal at 4 ps in functional reaction centers arises from bleaching which is mainly caused by the electrochromic shift of B after charge transfer.<sup>36</sup> Because pump and probe scattering

background increased as the pump power was increased, the true signal was obtained by subtracting the pump–probe background at 1 ps from the signal at 4 ps. The linear regression fit shown in the figure is of the form  $S = c(I/I_s) - c(I/I_s)^2$ , where  $c$  is a proportionality constant and  $I_s$  is a “saturation intensity”.<sup>51</sup> The least squares saturation intensity was 8 nJ (8 pJ/ $\mu\text{m}^2$  or  $3 \times 10^7$  photons/ $\mu\text{m}^2$ ). The fractional reduction in pump–probe signal due to saturation is given by  $I/(I + I_s)$ , so the pump–probe signal at 4 ps delay and 500 pJ pulse energy is reduced by 6% because of saturation. Pump–probe transients recorded at higher pulse energies exhibit a slower initial decay, a new exponential fit component which decays with  $\tau \approx 400$  fs, and a reduced amplitude for the 2.8 ps rise.<sup>40,45</sup>

**H. Anisotropy.** During pump–probe scans, the lock-in output (10 ms time constant) was sampled at intervals of 1 ms and 50 points were digitally averaged at each pump–probe delay. (This records a data point every five lock-in time constants so that scattering off a particle or bubble would affect only one data point.) Ten scans of the pump–probe delay were digitally averaged to record each data file. Scans covered pump–probe delays from 300 fs before time zero to 2–15 ps after time zero. The pump–probe delay intervals were shorter at earlier times in order to capture both the initial rapid decay and the long time dynamics on a single scan. Alternating between parallel, perpendicular, and magic angle pump–probe polarizations, 15 data files were recorded for each polarization. This rotation averaged the effects of sample degradation. After recording a complete set of 45 data files, the sample was removed, centrifuged, and filtered before recording another set of depolarization measurements. Because this changed the optical density of the sample slightly, different data sets were fit separately.

Smaller data sets were recorded at higher pump energies to measure saturation effects: it was found that the anisotropy  $r = (S_{\parallel} - S_{\perp})/(S_{\parallel} + 2S_{\perp})$  at the maximum of the pump–probe signal (which occurs *after* zero delay and should not be confused with the initial anisotropy) dropped from 0.374(12) at 500 pJ pump energy to 0.367(48) at 2 nJ pump energy and 0.328(15) at 4 nJ pump energy. These anisotropies can be fit to an empirical form  $r(I) = r_0(1 - (I/I_t)^2)$ , where  $r_0 = 0.377$  and  $I_t = 11.2$  nJ/pulse, and indicate that the measured anisotropies at 500 pJ pump energy are reduced about 1% by saturation. In slightly saturated preliminary experiments, we were unable to detect a change in the anisotropy when the flow direction was changed by 90°, thus ruling out systematic errors in the anisotropy through alignment by flow. Upon completion of reaction center measurements, the anisotropy of IR144, the pump–probe cross correlation, laser spectrum, and pump–probe overlap were remeasured to verify stability of the experiment throughout the measurements.

**I. Elimination of Scattering Points.** Comparison of multiple data files within a set of 15 allowed removal of discrepant data points obviously caused by scattering off particles or bubbles. At each pump–probe delay, data points more than three standard deviations from the mean for that delay were removed. A single data file in which scattering effects were removed was created by selecting the median data point of those remaining at each delay, yielding one data file for each polarization. This procedure for eliminating scatter off bubbles was checked for consistency by comparing sets of 15 data files recorded with slightly different sample concentrations (which result from centrifuging and filtering the reaction centers). Data obtained with 799 nm center wavelength are shown in Figure 7, while data obtained at 805 nm are shown in Figure 8.

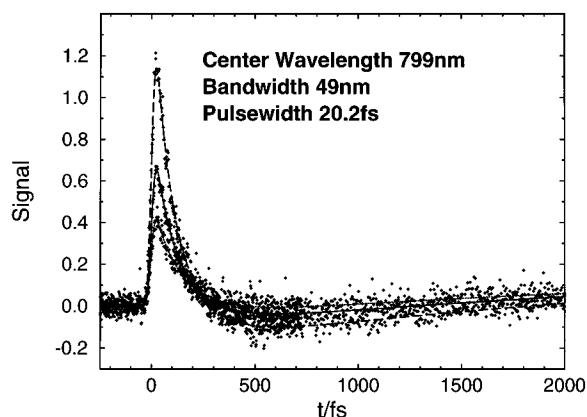


**Figure 7.** Transient absorption of *Rb. sphaeroides* R26 reaction centers recorded with 20.2 fs pump and probe pulses of 49 nm bandwidth (fwhm) centered at 799 nm. The signal was recorded with the probe polarization at parallel (long dashed line), perpendicular (dotted line), and magic angle (solid line) to the pump polarization. The pulse energy was 500 pJ, the spot size was 34  $\mu\text{m}$  1/e diameter, the repetition rate was 5 kHz, and the flow rate was  $\sim 100$  cm/s, which is sufficiently rapid to ensure that each sample volume was refreshed between pump pulses. The fit shown is the convolution of the autocorrelation with populations from a kinetic model in which energy is transferred from B to  $P_+$  (75 fs),  $P_+$  internally converts to  $P_-$  (165 fs), and  $P_-$  charge separates to form  $P^+H^-$  (2.7 ps).

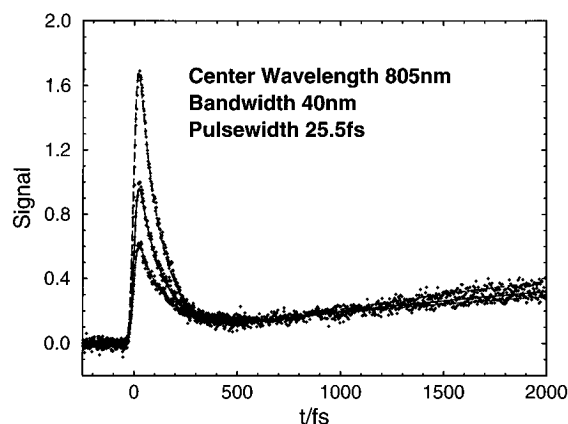


**Figure 8.** Transient absorption of *Rb. sphaeroides* R26 reaction centers recorded with 25.5 fs pump and probe pulses of 40 nm bandwidth (fwhm) centered at 805 nm. The signal was recorded with the probe polarization at parallel (long dashed line), perpendicular (dotted line), and magic angle (solid line) to the pump polarization. Other experimental conditions are given in Figure 4. The fit shown is the convolution of the autocorrelation with a kinetic model in which energy is transferred from B to  $P_+$  (85 fs),  $P_+$  internally converts to  $P_-$  (140 fs), and  $P_-$  charge separates to form  $P^+H^-$  (2.7 ps).

### III. Data Analysis

For preliminary analysis, the data files were individually fit to sums of exponentials convoluted with the instrument response function (the measured pump–probe cross-correlation). Results are presented in Table 1 for three data sets: scans recorded at 799 nm over  $-300$  fs to 15 ps; scans recorded at 805 nm over  $-300$  fs to 2 ps; and scans recorded at 805 nm over  $-300$  fs to 15 ps (this last set was constructed from five rather than 15 data files). Satisfactory fits to the 799 nm data set (magic angle data shown in Figure 4) required a rapidly decaying exponential, a slowly rising exponential, and an instantaneous baseline shift:

$$S = [A_1 \exp(-t/\tau_2) + A_2(1 - \exp(-t/\tau_2)) + A_3] \otimes \text{IRF} \quad (1)$$

The best fit parameters for the 799 nm magic angle data set are  $A_1 = 83\%$ ,  $\tau_1 = 124$  fs;  $A_2 = 26\%$ ,  $\tau_2 = 2.766$  ps, and  $A_3 = -9\%$ . The best fit parameters for all data sets are given in Table 1. Within each data set, the amplitudes in Table 1 are

**TABLE 1: Biexponential Fit Parameters from Eq 1 for Pump–Probe Transients on Isolated Reaction Centers from *Rb. sphaeroides*<sup>a</sup>**

	$A_1$	$\tau_1$ (fs)	$A_2$	$\tau_2$ (fs)	$A_3$
	805 nm, -0.3 to 15 ps				
magic angle	1.26	117	0.515	2280	0.02
	71%		29%		1%
parallel	2.22	110	0.691	2550	-0.02
	76%		24%		-1%
perpendicular	0.715	152	0.447	1970	0.03
	62%		38%		3%
	805 nm, -0.3 to 4 ps				
magic angle	1.23	123	0.636	2765 (fixed)	
	66%		34%		
parallel	2.22	106	0.747	2765 (fixed)	
	75%		25%		
perpendicular	0.697	155	0.561	2765 (fixed)	
	55%		45%		
	799 nm, -0.3 to 15 ps				
magic angle	0.956	124	0.294	2770	-0.1078
	83%		26%		-9%
parallel	1.69	110	0.388	3330	-0.1629
	88%		20%		-8%
perpendicular	0.568	140	0.232	2800	-0.05935
	77%		31%		-8%

<sup>a</sup> Within each data set, the amplitudes are given on the same scale to allow comparison of parallel, perpendicular, and magic angle signals. Relative percentages are given on the next line.

**TABLE 2: Anisotropies for Energy Transfer Steps Used in Fitting the Data to Eq 2**

step	anisotropy
B (initial)	0.4
B→P <sub>+</sub>	-0.07
B→P <sub>-</sub>	0.25
B→P <sup>+</sup> H <sup>-</sup>	floated
P <sub>+</sub> (initial)	0.4
P <sub>+</sub> →P <sub>-</sub>	-0.2
P <sub>+</sub> →P <sup>+</sup> H <sup>-</sup>	floated

given on the same scale to allow comparison of the experimental magnitudes of parallel, perpendicular, and magic angle pump–probe signals. Because a 400 fs decay had been observed after 800 nm excitation of B in all prior studies (including our own), the data were also fit with a sum of two exponential decays, a rise, and a baseline shift: when one time constant was set to 400 fs, the time constant either converged to the time constant  $\tau_1$  of the two exponential fit or the amplitude converged to zero. There was no improvement in the reduced  $\chi$ -squared. Exponential fitting does recover an  $\sim 400$  fs decay when either (1) the pulse energy is high enough to saturate; (2) the repetition rate is high enough to excite unrelaxed reaction centers; or (3) the special pair has been chemically oxidized. We conclude that the 400 fs decay is an artifact of double excitations.

The time constant  $\tau_2$  is consistent with previous measurements of the electron transfer rate from the lower exciton component of the special pair (P<sub>-</sub> → P<sup>+</sup>H<sup>-</sup>) by other techniques,<sup>3,52,53</sup> and it is known that electron transfer produces a bleach in the 800 nm region which has been assigned to an electrochromic blue shift of B.<sup>36</sup> The initial decay is associated with bleach recovery as B returns to its ground state after energy transfer, but a fit to the parallel pump–probe polarization scan yields  $\tau_1 = 110$  fs while the perpendicular polarization scan yields  $\tau_1 = 140$  fs (see Table 1). These differences indicate a rapid change in the anisotropy during the initial decay, which implies that an acceptor (not necessarily the initial acceptor) also absorbs light near 800 nm. This is not surprising, since the transition from the ground state of the special pair to the upper exciton state is centered around 810 nm so that the ground state of the special pair will be bleached upon energy transfer to either exciton

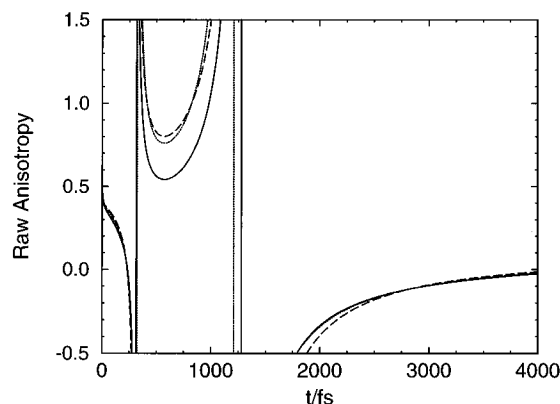


**Figure 9.** Raw anisotropy curves constructed from the fitted curves to the parallel, perpendicular and magic angle data in Figure 8. The fitting functions were sums of exponentials convoluted with the autocorrelation (eq 1). The anisotropy curves shown are constructed from all double combinations of parallel, perpendicular, and magic angle pump–probe scans using eq 4: parallel and magic angle (solid line); magic angle and perpendicular (long-dashed line); parallel and perpendicular (dotted line). The raw (i.e., not deconvoluted) initial anisotropy value approaches 0.4.

component of P. Since P also absorbs near 800 nm, the decay of the magic angle signal cannot be ascribed entirely to recovery of ground state B and cannot be directly interpreted as an energy transfer rate.

The pump–probe anisotropy calculated from the exponential fits is shown in Figure 9. Note that the initial raw anisotropy is approximately 0.4 and that very large effective anisotropies are observed at some times. Use of the parameters  $A_1$  and  $A_3$  from Table 1 allows calculation of the deconvoluted initial anisotropy  $r(0)$ . For the 805 nm data, we obtain  $r(0) = 0.391(27)$ , while the 799 nm data sets yield  $r(0) = 0.420(13)$  and  $r(0) = 0.401(1)$ .

The presence of an acceptor which absorbs at 800 nm is also implied by the negative pump–probe signal between 200 fs and 1 ps delay. A negative pump–probe signal means that the pump pulse has increased the absorbance of the sample. Since electronically excited monomeric bacteriochlorophyll does not absorb light at 800 nm, the simplest explanation of this absorbance increase is that the excited state of an acceptor absorbs light near 800 nm. It is therefore necessary to include absorption by electronically excited states of the reaction center in a model to determine the energy transfer mechanism from the pump–probe anisotropy data.

#### IV. Pump–Probe Depolarization

The pump–probe signal is the pump-induced change in the probe beam intensity transmitted through the sample. We have experimentally defined a pump-induced increase in sample transmittance (a bleach) as a positive pump–probe signal. For simplicity, we have used kinetic models in fitting our data. It is assumed that energy is transferred between pigments according to rate equations and that the reaction center does not reorient on the time scale of the electronic energy transfer. The time-dependent signal when pigment  $i$  is initially excited is then given by a sum of pump–probe signals from each pigment  $j$  to which energy has been transferred,

$$S_i(t) = \sum_j S_j P_j(t) (1 + f_{\text{pol}} r(\theta_{ij})) \quad (2)$$

where  $S_j$  is the strength of probe absorption by pigment  $j$  (roughly determined by the overlap of the absorption and emission spectra of pigment  $j$  with the probe frequency spectrum),  $P_j(t)$  is the time-dependent population of the elec-

tronically excited state of pigment  $j$ ,  $f_{\text{pol}}$  is a function of the angle between the pump and probe laser polarizations, and  $r$  is the polarization anisotropy which depends on the angle  $\theta_{ij}$  between the transition dipole moment of the initially excited pigment  $i$  and the transition dipole moment of the pigment  $j$  to which energy has been transferred through the equation

$$r(\theta_{ij}) = \frac{1}{5}(3 \cos^2(\theta_{ij}) - 1) \quad (3)$$

The function  $f_{\text{pol}}$  takes on the values  $+2$  for parallel pump and probe polarizations,  $0$  for pump and probe polarizations at the “magic angle”, and  $-1$  for perpendicular pump and probe polarizations. The anisotropy can thus be measured as either

$$r = \frac{S_{\parallel} - S_{\perp}}{S_{\parallel} + 2S_{\perp}}, \quad r = \frac{S_{\text{MA}} - S_{\perp}}{S_{\text{MA}}}, \quad \text{or} \quad r = \frac{S_{\parallel} - S_{\text{MA}}}{2S_{\text{MA}}} \quad (4)$$

For nondegenerate dipole transitions in isolated molecules, the initial anisotropy  $r(0) = 2/5$ , and the fluorescence anisotropy can vary between  $-1/5$  and  $2/5$  (the limits given by eq 3) as the dipoles realign.<sup>54</sup> Anisotropies between  $-1/2$  and  $1$  have been found in theoretical work on coherent superpositions of transition moments.<sup>55–60</sup> There is another way anisotropies outside the usual range can occur. The anisotropy has the property that if the signal is a sum,  $S_{\text{pp}} = \alpha I_{\text{A}} + \beta I_{\text{B}}$ , then the observed anisotropy is an average  $r_{\text{pp}} = (\alpha/(\alpha + \beta))r_{\text{A}} + (\beta/(\alpha + \beta))r_{\text{B}}$ . The signal in pump–probe spectroscopy is a sum of signals from three sources: positive signals from ground state depletion, positive signals from excited state stimulated emission, and negative signals from excited state absorption.<sup>61,62</sup> In the presence of both positive and negative signals, the pump–probe anisotropy can take on any value,  $-\infty < r_{\text{pp}} < \infty$ .

## V. Electronic Structure of the Reaction Center

In order to determine the energy transfer kinetics from the pump–probe depolarization transients, it is necessary to know the frequencies and transition moments for ground state absorption, excited state stimulated emission, and excited state absorption for the various pigments in the reaction center. These frequencies and transition moments depend on the coupling between pigments. Won and Friesner<sup>21–23</sup> developed an effective Hamiltonian for bacterial reaction centers which includes both changes in geometry upon electronic excitation and Förster dipole–dipole excitonic coupling between pigments. Lathrop and Friesner<sup>24</sup> have determined the parameters of this Hamiltonian for *Rb. sphaeroides* by modeling several spectroscopic experiments (absorption spectra, circular dichroism spectra, Resonance Raman spectrum of  $\text{P}^*$ , photochemical hole burning, Stark spectra). Frequencies and transition dipoles for ground state absorption and excited state stimulated emission are taken from the Hamiltonian of Lathrop and Friesner. In addition, we have used a similar effective Hamiltonian to model the absorption spectra of the excited states of the special pair. In this section, we discuss the three types of pump–probe signals from the photosynthetic reaction center.

The special pair forms a strongly coupled bacteriochlorophyll dimer. In the absence of excitonic coupling, the two bacteriochlorophylls in the special pair would have nearly degenerate  $\text{Q}_y$  electronic states (both lowered in energy by the protein environment). Resonant excitonic coupling between the two  $\text{Q}_y$  excited states in the special pair yields symmetric ( $\text{P}_+$ ) and antisymmetric ( $\text{P}_-$ ) electronic states of the dimer which are delocalized over both bacteriochlorophylls. When chromophores are excitonically coupled, excitation of one electronic transition can change the entire electronic spectrum. The changes in the spectrum upon excitation of one electronic

transition are predictable if we can ignore all electronic states in which any bacteriochlorophyll is excited to a state other than  $\text{Q}_y$ . Since the laser spectrum overlaps the  $\text{Q}_y$  band exclusively, the experiment is insensitive to changes outside the  $\text{Q}_y$  region and such predictions are useful. Below, we discuss the changes in the electronic spectrum upon  $\text{Q}_y$  excitation on the assumption that the two B's are not coupled to each other or the special pair. Calculations which find appreciable excitonic coupling between  $\text{B}_L$  and  $\text{B}_M$  indicate that they are primarily mixed with  $\text{P}_+$ .<sup>21–24,63</sup> Since the laser spectrum covers both B and  $\text{P}_+$  absorption, the experiment is relatively insensitive to the extent of coupling between these pigments, so coupling among  $\text{B}_L$ ,  $\text{B}_M$ , and  $\text{P}_+$  is neglected entirely to simplify the discussion.

**A. Ground State Bleach.** The excitonic coupling between the two bacteriochlorophylls of the special pair implies that the special pair can be thought of as a single molecule with one ground state and two singly excited  $\text{Q}_y$  states ( $\text{P}_+$  and  $\text{P}_-$ ). Excitation of either  $\text{P}_+$  or  $\text{P}_-$  will depopulate the ground state, which is common to both, and bleach all transitions originating from the ground state. This implies that excitation of  $\text{P}_+$  with 810 nm light contributes instantaneous absorbance decreases to the experimental pump–probe signals at both 810 nm (dipole  $\mu_{\text{P}_+}$ , anisotropy  $r = 0.4$ ) and 870 nm (dipole  $\mu_{\text{P}_-}$ , anisotropy  $r = -0.2$ ) by depopulating the ground state of P. Similarly, excitation of  $\text{P}_-$  with 870 nm light instantly depopulates the ground state of P and contributes absorbance decreases at both 870 nm (dipole  $\mu_{\text{P}_-}$ , anisotropy  $r = 0.4$ ) and 810 nm (dipole  $\mu_{\text{P}_+}$ , anisotropy  $r = -0.2$ ). *These instantaneous induced bleaches are simply “V” configuration double resonance signals<sup>51</sup> and do not represent energy transfer between exciton states.* Unless the bleach rise is clearly resolved, an “instantaneous” bleach may indicate either excitonic coupling between pigments, electronic transitions which belong to the same pigment, or energy transfer.

**B. Stimulated Emission.** Stimulated emission signals are more straightforward than ground state bleach signals. The absorbance decreases due to stimulated emission occur only when the emitting chromophore is electronically excited. Therefore, observations of emission from one electronic state after excitation of another are always indicative of energy transfer or internal conversion. Laser pulses near 800 nm can stimulate emission from B and possibly from  $\text{P}_+$  with the same transition dipole moments as the corresponding absorption transitions.

**C. Excited State Absorption.** To first order, the  $\text{Q}_y$  transitions of the ground state determine the  $\text{Q}_y$  transitions from the singly excited states of the dimer. This is most easily seen by introducing a site-localized basis in which the transition moments are known and deriving the transition moments of the dimer by taking appropriate linear combinations of site-localized basis states. The energies and transition moments of the special pair dimer in the site localized basis are shown schematically in Figure 10. The ground electronic state  $\text{g}_{\text{LGM}}$  of the special pair is taken as the zero of energy. The two singly excited states  $\text{e}_{\text{LGM}}$  ( $\text{P}_L$  excited) and  $\text{g}_{\text{LEM}}$  ( $\text{P}_M$  excited) are both assumed to have the same energy  $E$  (this simplifying assumption is not necessary). The two singly excited states are excitonically coupled to each other by an off-diagonal matrix element  $V$  ( $V > 0$ ). The doubly excited state  $\text{e}_{\text{LEM}}$  ( $\text{P}_L$  and  $\text{P}_M$  each singly excited) has energy  $2E$ . In the site basis, the electric dipole transition moments are  $\langle \text{e}_{\text{LGM}} | \mu | \text{g}_{\text{LGM}} \rangle = \mu_L$ ,  $\langle \text{g}_{\text{LEM}} | \mu | \text{g}_{\text{LGM}} \rangle = \mu_M$ ,  $\langle \text{e}_{\text{LEM}} | \mu | \text{e}_{\text{LGM}} \rangle = \mu_M$ , and  $\langle \text{e}_{\text{LEM}} | \mu | \text{g}_{\text{LEM}} \rangle = \mu_L$ , where  $\mu_L$  is the  $\text{Q}_y$  transition dipole moment vector of  $\text{P}_L$  and  $\mu_M$  is the  $\text{Q}_y$  transition dipole moment vector of  $\text{P}_M$ .

Diagonalization of this effective Hamiltonian yields two excitonically coupled eigenstates,  $\text{P}_+$  (approximate energy  $E$ )

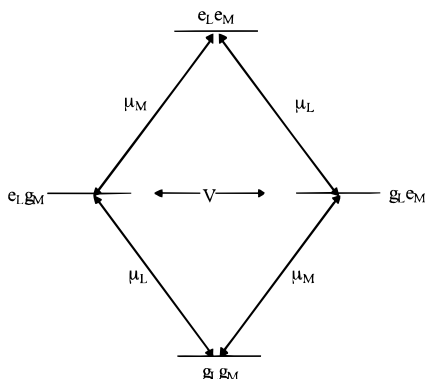


**Figure 10.** Four states of the special pair dimer in the site basis. The ground electronic state  $g_L g_M$  of the special pair is taken as the zero of energy. The two singly excited states  $e_L g_M$  ( $P_L$  excited) and  $g_L e_M$  ( $P_M$  excited) are both assumed to have the same energy  $E$  (this simplifying assumption is not necessary). The two singly excited states are excitonically coupled to each other by an off-diagonal matrix element  $V$  ( $V > 0$ ). The doubly excited state  $e_L e_M$  ( $P_L$  and  $P_M$  each singly excited) has energy  $2E$ . In the site basis, the electric dipole transition moments are  $\langle e_L g_M | \mu | g_L g_M \rangle = \mu_L$ ,  $\langle g_L e_M | \mu | g_L g_M \rangle = \mu_M$ ,  $\langle e_L e_M | \mu | e_L g_M \rangle = \mu_M$ , and  $\langle e_L e_M | \mu | g_L e_M \rangle = \mu_L$ , where  $\mu_L$  is the  $Q_y$  transition dipole moment vector of  $P_L$  and  $\mu_M$  is the  $Q_y$  transition dipole moment vector of  $P_M$ .

+  $V$ ) and  $P_-$  (approximate energy  $(E - V)$ ) with eigenvectors

$$|P_+\rangle = (1/\sqrt{2})|e_L g_M\rangle + (1/\sqrt{2})|g_L e_M\rangle \quad (5)$$

$$|P_-\rangle = (1/\sqrt{2})|e_L g_M\rangle - (1/\sqrt{2})|g_L e_M\rangle \quad (6)$$

Because  $V$  is positive,  $P_-$  lies energetically below  $P_+$ . The transition dipole matrix elements for the excitonically coupled states may be obtained from those in the site basis, e.g.,  $\langle P_+ | \bar{\mu} | g_L g_M \rangle = (1/\sqrt{2})(\langle e_L g_M | \bar{\mu} | g_L g_M \rangle + \langle g_L e_M | \bar{\mu} | g_L g_M \rangle) = (1/\sqrt{2})(\bar{\mu}_L + \bar{\mu}_M)$  so that  $\langle P_- | \bar{\mu} | g_L g_M \rangle = (1/\sqrt{2})(\bar{\mu}_L - \bar{\mu}_M)$ ,  $\langle P_- | \bar{\mu} | e_L e_M \rangle = -(1/\sqrt{2})(\bar{\mu}_L - \bar{\mu}_M)$ , and  $\langle P_+ | \bar{\mu} | e_L e_M \rangle = (1/\sqrt{2})(\bar{\mu}_L + \bar{\mu}_M)$ . The spectroscopic transition frequencies are determined from the energy level differences between eigenstates. We thus obtain the result that the excited state absorption  $P_- \rightarrow e_L e_M$  is centered at 810 nm with the same transition dipole moment alignment  $\pm(\bar{\mu}_L - \bar{\mu}_M)$  as the  $g_L g_M \rightarrow P_-$  transition while the absorption from  $P_+ \rightarrow e_L e_M$  is centered at 870 nm with the same transition moment  $(1/\sqrt{2})(\bar{\mu}_L + \bar{\mu}_M)$  as the  $g_L g_M \rightarrow P_+$  transition.

This model neglects interactions between the singly excited states and the charge transfer state of the special pair,<sup>18–20,24,64</sup> but it can be shown that the zero electric dipole transition moments between the charge transfer state and the ground state and doubly excited state allow these interactions to be correctly incorporated by using transition moments from an effective Hamiltonian which includes these interactions (e.g., that of Lathrop and Friesner<sup>24</sup>) while maintaining the relationships between transition moments given above. There are also excitonic interactions between the doubly excited states in which each chromophore is singly excited and the doubly excited states in which one chromophore is doubly excited, but these are probably nonresonant, in which case they can be neglected. When  $P_-$  is excited directly at 870 nm, it has been observed<sup>65</sup> that there is an instantaneous absorbance increase at 800 nm, as predicted by the above model. (The net experimental absorbance increase at 800 nm is the sum of an absorbance increase due to  $P_- \rightarrow P^{**}$  excited state absorption and an absorbance decrease due to ground state bleaching of the  $P \rightarrow P_+$  transition upon excitation of  $P_-$ .) The above model can also be applied to the structurally similar B800–850 dimer in LH2

**TABLE 3: Transition Moments for Ground State Bleaching, Stimulated Emission, and Excited State Absorption Terms in the Pump–Probe Signal Near 800 nm for Each Chromophore<sup>a</sup>**

	bleach	emission	induced absorption
$B_L$	$\mu_L$	$\mu_L$	0
$B_M$	$\mu_M$	$\mu_M$	0
$P_+$	$\mu_+$	$\mu_+$ (?)	0
$P_-$	$\mu_+$	0	$\mu_-$

<sup>a</sup> A question mark is placed by the emission dipole for  $P_+$  because it is not clear if stimulated emission from  $P_+$  overlaps the laser spectrum

and explains the observation that the excited state of B850 absorbs at 800 nm.<sup>66–68</sup>

The absorbance changes expected at 800 nm upon excitation of the various pigments are summarized in Table 3.

## VI. Kinetic Models

Modeling the energy transfer in the reaction center poses a theoretical challenge: the  $\sim 100$  fs time scales involved strongly suggest that the energy transfer is at least partially electronically coherent, given that the minimum electronic dephasing time scale is  $T_2 \geq (1/\pi\Delta\nu) = 20$  fs. Theory<sup>55–58</sup> indicates that the initial pump–probe anisotropy should be 0.50 for coherent excitation of the two B chromophores, while the experimental initial anisotropy closely matches the value of 0.4 expected for incoherent excitation. In the absence of theoretically expected signs of electronic coherence, we attempted to fit the parallel, perpendicular, and magic angle data simultaneously<sup>69</sup> by feeding populations from simple kinetic models into eq 2 and convoluting with the instrument response function. The goal was to use anisotropies calculated from the reaction center structure to determine electronic state populations during the energy transfer process. We doubt the kinetic rates have a physical significance beyond producing sensible time-dependent electronic state populations and have not refined the kinetic model because we think a quantum description of energy transfer which involves competition between interchromophore electronic coupling and electronic dephasing would be more realistic.<sup>70–72</sup> For this reason and because we are resolving only a single time scale per energy transfer step, we have also excluded from consideration kinetic schemes involving reversible steps.

The anisotropies between relevant transition dipole pairs in Table 2 were fixed in fitting all models. Because the 800 nm band has not been unambiguously separated into contributions from the various pigments at room temperature, the strength of each transition ( $S_j$  in eq 2) was allowed to float with the idea that the fitted strengths could be used as a check on the kinetic model. The strengths included are motivated by the list in Table 3. Absorption and emission strengths from each chromophore were lumped together into a single bleach term (e.g.,  $S_{P_+}$ ). The strengths for  $B_L$  and  $B_M$  were taken to be identical ( $S_B$ ). It is unclear to what extent the laser spectrum stimulates emission from  $P_+$ , since emission is probably Stokes shifted to the red of 810 nm by vibrational displacements. We have therefore fit the data twice: one fit assumed no stimulated emission from  $P_+$ ; the other fit assumed that the emission and absorption spectra are identical and contribute equally to the  $P_+$  bleach. These two assumption produce slightly different results for other fit parameters because the ground state absorption of  $P_+$  is bleached when either  $P_+$  or  $P_-$  is excited, but  $P_+$  emission cannot occur from  $P_-$ . Two electronic transitions with different directions originate from  $P_-$ : a ground state bleach of the  $P_+$  absorption and a  $P_-$  excited state absorption ( $S_{P_-}$ ) which was allowed to float. If the laser spectrum cannot stimulate emission

**TABLE 4: Best Fit Parameters Obtained in Fitting the Data to Eq 2 Using the Kinetic Model of Eq 9**

	$S_B^a$	$\tau_{B \rightarrow P_+}$ (fs)	$S_{P_+}$	$\tau_{P_+ \rightarrow P_-}$ (fs)	$S_{P_-}$	$\tau_{CS}^d$ (ps)	$S_{P^+H^-}$	$F$	$r_{B \rightarrow P^+H^-}$	$r_{P_+ \rightarrow P^+H^-}$
First Parameter Set <sup>b</sup>										
799 nm	1	75	0.211	165	-0.289	2.7	0.171	0.225	0.142	-0.2 <sup>c</sup>
805 nm	1	83	0.245	142	-0.208	2.7	0.376	0.283	0.283	-0.199
Second Parameter Set <sup>d</sup>										
799 nm	1	83	0.160	177	-0.171	2.7	0.202	0.051	0.091	-0.2 <sup>c</sup>
805 nm	1	92	0.201	145	-0.057	2.7	0.421	0.159	0.220	-0.2 <sup>c</sup>

<sup>a</sup> The parameters  $S_B$  and  $\tau_{CS}$  were fixed. <sup>b</sup> The first parameter set assumes large  $P_+$  Stokes shift and no  $P_+$  stimulated emission. <sup>c</sup> The anisotropy  $r_{P_+ \rightarrow P^+H^-}$  converged to the lower limit allowed by the fit. <sup>d</sup> The second parameter set is from a fit assuming zero  $P_+$  Stokes shift and perfect overlap between  $P_+$  absorption and emission spectra.

from  $P_+$  (first fit assumption), the strength of the  $P_-$  ground state bleach is equal to the strength of the  $P_+$  bleach ( $S_{P_+}$ ), which arises entirely from ground state depopulation. If the absorption and emission spectra overlap perfectly and have equal strength (second fit assumption), then the strength of the  $P_-$  ground state bleach should be one-half the strength of the  $P_+$  bleach ( $S_{P_+}/2$ ) since there is no  $P_+$  emission from  $P_-$ . For the bleach produced by charge separation, both the strength  $S_{P^+H^-}$  and the anisotropies were allowed to float.

The anisotropy of each relevant transition dipole pair was calculated from the direction of the  $Q_y$  transition moments<sup>21</sup> and the electronic eigenvectors<sup>63</sup> available for *Rhodospseudomonas viridis*. El-Kabbani et al.<sup>6,7</sup> have discussed the differences between the *Rb. sphaeroides* and *Rps. viridis* reaction centers. The initial anisotropy of B and  $P_+$  were taken to be 0.4. Other anisotropy values were calculated (using eq 3) from the angle between the initially excited transition dipole and the transition dipole probed after energy transfer. The B to P anisotropies were dipole strength weighted averages and were calculated using the excitonically coupled states of Won and Friesner, e.g.  $r_{B \rightarrow P_+} = (D_{B_+} r_{B_+ \rightarrow P_+} + D_{B_-} r_{B_- \rightarrow P_+}) / (D_{B_+} + D_{B_-})$ , where  $D$  is the dipole strength. This calculation assumes that there is no electronic coherence between the two excited states of B and yields slightly different results for monomeric B ( $r_{B \rightarrow P_+} = -0.11$  vs  $-0.07$  and  $r_{B \rightarrow P_-} = 0.27$  vs  $0.25$ ). The anisotropies for energy transfer to the charge separated state  $P^+H^-$  were allowed to vary within a range of  $-0.2$  to  $0.4$  because the electrochromic band shift is expected to be greater for  $B_L$  than  $B_M$  and because the electronic transition of the oxidized special pair is insufficiently characterized.

We first attempted to fit the data to a crude two-step three-state model where energy is transferred directly from B to  $P_-$  followed by charge separation to  $P^+H^-$



When this model was unable to reproduce the rapid drop in the anisotropy, we included an adjustable fraction  $F = N_{P_+}(0) / (N_{B-}(0) + N_{P_+}(0))$  of direct  $P_+$  excitation through the absorption band at 810 nm and assumed that this fraction internally converts to  $P_-$  before charge separation:



This model was capable of producing a rapid anisotropy drop but yielded discrepant internal conversion time constants (30 fs for a 15 ps scan at 805 nm vs 560 fs for a 4 ps scan at 805 nm) and frequently failed to converge. The fitted fraction ( $F \approx 0.02$ ) of initially excited  $P_+$  disagreed with that expected on the basis of the fitted strengths ( $S_{P_+} / (S_B + S_{P_+}) \approx 0.17$ ). Upon close visual inspection, we were not satisfied with the quality of the fit. Finally, we turned to a four-state three-step model

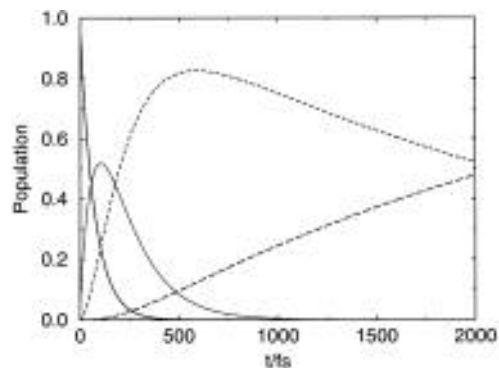
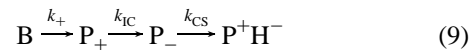


**Figure 11.** Normalized state populations from the kinetic model of eq 9 as a function of time. In the calculation shown here, all excitation starts on B at time zero. Energy transfer from B to  $P_+$  is followed by internal conversion between  $P_+$  and  $P_-$ , which subsequently charge separates to produce  $P^+H^-$ : (B) solid curve; ( $P_+$ ) dotted curve; ( $P_-$ ) short dashed curve; ( $P^+H^-$ ) long dashed curve.

in which B transfers energy to  $P_+$ ,  $P_+$  internally converts to  $P_-$ , and  $P_-$  charge separates to form  $P^+H^-$ :



where again the fraction of initially excited  $P_+$  internally converts to  $P_-$  before charge separation. The fits to the solution of kinetic scheme 9 were judged to be satisfactory, and the best fit parameters for two fits are given in Table 4. The upper set of parameters in Table 4 is based on the assumption that the  $P_+$  emission spectrum is Stokes shifted so that the overlap with the laser spectrum is zero, while the lower set of parameters assumes that the Stokes shift is zero and the absorption and emission spectra overlap perfectly. These two extreme assumptions both lead to reasonable fits with similar parameters, although the fit is slightly better for the assumption of no  $P_+$  stimulated emission. The real Stokes shift should lie between these extremes and should also fit the kinetic model reasonably well. Note that the three-state scheme of eq 9 and the two-step scheme of eqs 7 and 8 both require specification of three rates, four strengths, two anisotropies, and the fraction of direct  $P_+$  excitation. This total of 10 parameters is less than the 15 parameters required to fit a set of parallel, perpendicular, and magic angle scans using eq 1. The time-dependent populations which result from these kinetic schemes are shown in Figure 11. Figures 7 and 8 show the data and fits (upper set of parameters in Table 4) for the 799 and 805 nm sets, respectively. The fit results were consistent between the data sets, and the amplitudes reflect the expected differences between the excitation pulses. When emission from  $P_+$  was assumed to be absent, the time constants for the 799 nm (805 nm) transfer rates were as follows: energy transfer from B to  $P_+$   $\tau_{B \rightarrow P_+} = 75$  fs (85 fs); internal conversion from  $P_+$  to  $P_-$   $\tau_{P_+ \rightarrow P_-} = 165$  fs (140 fs); the time constant for the electron transfer from  $P_-$  to  $P^+H^-$  was fixed at 2.7 ps for both data sets. The fitted strengths for

the 799 nm (805 nm) data sets were the following:  $S_B = 1$  (fixed);  $S_{P_+} = 0.21$  (0.24);  $S_{P_-} = -0.29$  (-0.21);  $S_{P^+H^-} = 0.17$  (0.38). The fraction of initially excited  $P_+$  was  $F = 0.23$  (0.28), in reasonable agreement with the fraction expected from the fitted strengths 0.17 (0.19). Slight differences are expected because both absorption and emission from B contribute to  $S_B$ . The qualitative trends in the lower parameter set (which includes  $P_+$  emission) are similar, although the strengths for  $P_+$  and  $P_-$  are lower. There is an apparent discrepancy between  $F$  and  $(S_{P_+}/S_B + S_{P_+})$  for the 799 nm data set, but  $F$  is too poorly determined to establish a disagreement. In both fits, the anisotropies  $r(P_+ \rightarrow P^+H^-)$  and  $r(B \rightarrow P^+H^-)$  are strongly correlated and  $r(P_+ \rightarrow P^+H^-)$  is not well determined: however, the convergence of one fit to  $r(P_+ \rightarrow P^+H^-) = -0.199$  suggests convergence to the lower limit ( $r = -0.2$ ) may represent the correct anisotropy for this energy transfer step. Compared to the direct energy transfer model (eqs 7 and 8), the kinetic scheme of eq 9 improved the reduced  $\chi$ -squared of the fit for all three data sets. The 799 nm data included more scattering which tends to produce a positive signal so that the residuals were slightly biased both before and after time zero. Except for the presence of oscillations in the early portion of the signal (see below) fits to the 805 nm data converged to within our ability to estimate the errors.

Figure 2 shows overlap of the initial excitation pulses with the steady state absorption spectrum of the reaction center. The region of different spectral overlap between the 799 and 805 nm pump-probe pulses should more or less represent the differences in strengths for the various states used in the fits. The main trends in the strengths are qualitatively as expected: compared to the 805 nm pulse, the 799 nm pulse overlaps less with the  $P_+$  spectrum so both  $F$  and  $S_{P_+}$  are lower at 799 nm; the special pair excited state absorption increase peaks at  $\approx 795$  nm (see Figure 2 of ref 65), so  $S_{P_-}$  is larger at 799 nm than 805 nm; the electrochromic blue shift of B causes less overlap (hence more bleaching) for the 805 nm pulse, so that  $S_{P^+H^-}$  is significantly larger at 805 nm. These strengths are in rough accord with estimates based on overlap between the laser spectrum and a Gaussian decomposition of the room temperature spectrum using the transition strengths and center frequencies from Won and Friesner.<sup>21-24</sup> The 799 nm center frequency pulse is expected to excite 59% B, 24%  $P_+$ , 12% H, and 5%  $P_-$  while the 805 nm pulse should excite 61% B, 27%  $P_+$ , 6% H, and 5%  $P_-$ . The fractional excitation of H and  $P_-$  is small enough to be neglected.

The initial anisotropy of B was investigated carefully because of the theoretically calculated<sup>55-58</sup> initial anisotropy of 0.50 for a dimer with a  $134^\circ$  angle between transition dipoles. It should be noted that the calculated anisotropy is independent of the excitonic coupling strength. Fits to the data with an initial anisotropy of B fixed at 0.5 were unsatisfactory. Fits where the anisotropy of B was allowed to float starting from 0.5 converged to 0.39. These results are not surprising given the raw initial anisotropy of nearly 0.4 in Figure 9 and the deconvoluted value of  $r(0) = 0.404(15)$  given by the fits to eq 1. Accounting for a 1% reduction in the initial anisotropy due to saturation, the observed initial anisotropy is, within experimental error, equal to  $2/5$ , the value expected for excitation of a single dipole. We are uncertain why the experimental initial anisotropy disagrees with that calculated from the theory for coherent excitation of reaction center chromophores.

The anisotropy of the bleach created upon charge separation is somewhat difficult to estimate theoretically. It is expected that the electrochromic shift will be larger for  $B_L$  than for  $B_M$  because the electron is transferred to  $H_L$ . The transition to the upper exciton state of the special pair at 810 nm is evidently

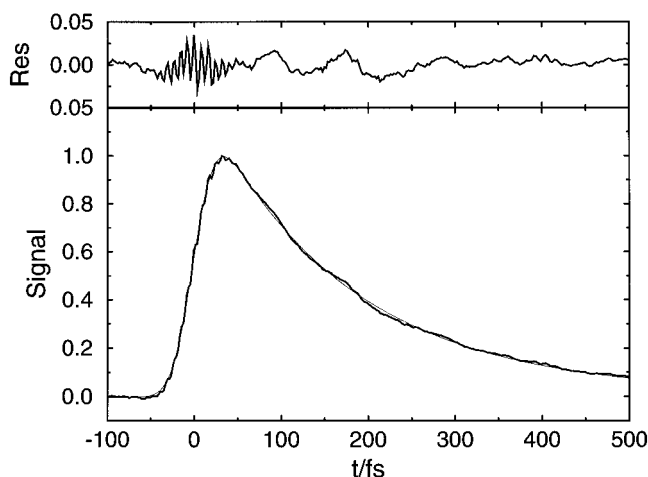


**Figure 12.** Parallel pump-probe signal for reaction centers recorded using 27 fs pulses at 803 nm center wavelength with 38 nm bandwidth. This transient was *not* recorded under single excitation conditions: 2 nJ pulse energy; 70  $\mu\text{m}$  beam diameter; 50 cm/s flow velocity; 152 kHz repetition rate. Quantum beat oscillations in the bleach decay can be clearly seen in the raw signal (heavy line). An exponential fit (light line) is shown to guide the eye. The upper panel shows residuals from the exponential fit.

replaced by a transition of the special pair cation, which Reimers and Hush place at about 847 nm by Gaussian fitting.<sup>73</sup> Our fitting procedure used two variable anisotropies  $r(B \rightarrow P^+H^-)$  and  $r(P_+ \rightarrow P^+H^-)$ . The fitted values are  $r(B \rightarrow P^+H^-) = 0.14$  (0.28) and  $r(P_+ \rightarrow P^+H^-) = -0.20$  (-0.199), which seem very roughly consistent with an electrochromic shift of  $B_L$  alone  $r(B \rightarrow B_L) = (r(B_L \rightarrow B_L) + r(B_M \rightarrow B_L))/2 = 0.25$  and  $r(P_+ \rightarrow B_L) = r(B \rightarrow P_+) = -0.07$ . The changes in the spectrum upon charge separation are almost certainly more complicated than a simple bleach of  $B_L$  alone and need to be better characterized for more detailed interpretation of the data.

## VII. Quantum Beats

Careful inspection of higher signal to noise data obtained previously at 152 kHz<sup>45</sup> reveals oscillatory behavior in the rapidly decaying portion (see Figure 12). These same oscillations are also present (but less clearly) in the lower signal to noise data at 5 kHz. Oscillations visible in the residuals were averaged over a 10 fs window for the parallel, perpendicular, and magic angle sets and fit with linear prediction starting 20 fs after time zero. Figure 13 shows the fit overlaying the residuals of the individual polarizations and their average. All three sets of residuals are shown on the same scale in Figure 13, and the oscillations are roughly the same magnitude in all three, indicating that the oscillations have near-zero anisotropy. Linear prediction analysis of the residuals yields frequency components of  $\sim 60\%$  relative amplitude at  $125\text{ cm}^{-1}$  and  $\sim 40\%$  relative amplitude at  $227\text{ cm}^{-1}$  decaying with time constants of 227 and 90 fs, respectively. The uncertainties in these frequencies and decay constants are rather large because they are distorted by the exponential fits.

In principle, quantum beats can originate from either electronic or vibrational coherence. Unless the two transition moments are nearly parallel, electronic quantum beats will produce oscillations in the anisotropy. The frequencies may be compatible with electronic quantum beats between states of B and  $P_+$ : of these, the only pair with nearly parallel transition dipoles is  $P_+$  and  $B_+$  (the symmetric state of excitonically coupled B). Another possibility is that the quantum beats are vibrational. In this case the anisotropy is determined by the energy transfer pathway. Examination of Table 2 reveals that only  $B \rightarrow P_+$  energy transfer can yield a near-zero anisotropy ( $r = -0.07$ ). The next lowest anisotropies in Table 2 can be

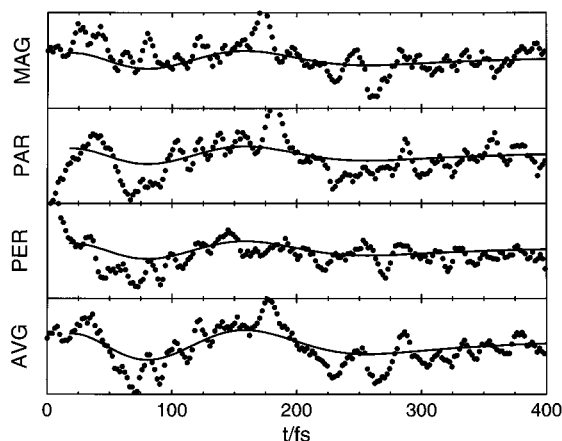


**Figure 13.** Magic angle, parallel, and perpendicular residuals from the fit to the kinetic scheme of eq 9 and their average. All residuals are shown on the same absolute scale and were smoothed over a 10 fs window. The solid line is a linear prediction fit of the average of all three sets of residuals which yields cosine frequencies of  $125\text{ cm}^{-1}$  ( $\sim 60\%$  relative amplitude) and  $227\text{ cm}^{-1}$  ( $\sim 40\%$  relative amplitude) decaying with time constants of 227 and 90 fs, respectively.

excluded as possibilities because they would yield parallel oscillations twice as strong as perpendicular ( $r = 0.25$ ) or perpendicular oscillations twice as strong as parallel ( $r = -0.2$ ). Vibrational quantum beats are not expected upon optical excitation of B because of the wide spectral bandwidth of the pulses and the small geometry change upon electronic excitation.<sup>62</sup> However, an  $\sim 80\text{ fs}$   $B \rightarrow P_+$  energy transfer step is fast enough to create vibrational wave packets of these frequencies upon excitation of the upper exciton component of the special pair in much the same way as a short optical pulse.<sup>61,62</sup> It is not clear from our data alone whether these wave packets are created in the upper exciton state or the ground state of the special pair.<sup>61,62</sup> The decay constants are consistent with either hypothesis. The  $125\text{ cm}^{-1}$  frequency is similar to that for quantum beats found in stimulated emission,<sup>74–76</sup> spontaneous emission,<sup>41</sup> resonance Raman spectra,<sup>77,78</sup> and hole-burning studies<sup>79</sup> of the lower exciton state of the special pair. Several workers have assigned this frequency to the interdimer vibration of the special pair because it is not observed in monomeric bacteriochlorophyll. Because the change in vibrational frequency for this mode between the ground and lower exciton states is small, it is likely that a similar frequency would also be prominent upon abrupt excitation of the upper exciton component of the special pair. The  $227\text{ cm}^{-1}$  frequency could represent the second harmonic<sup>61,74,80</sup> of the  $125\text{ cm}^{-1}$  mode of the special pair or a  $204\text{ cm}^{-1}$  vibration common to both P and B.<sup>78</sup> We are inclined to favor the hypothesis of vibrational quantum beats because it explains the presence of two beat frequencies. Regardless of their origin, the near-zero anisotropy supports  $P_+$  as the initial energy transfer acceptor.

### VIII. Discussion and Conclusions

From our studies of saturation, it is clear that very low photon fluxes (well below the saturation intensity of  $3 \times 10^7\text{ photons}/\mu\text{m}^2$ ) are necessary to obtain undistorted kinetics for the photosynthetic reaction center. This conclusion is not new. Several previous studies have reported a reduction of the charge transfer quantum yield at similar photon fluxes.<sup>35,81</sup> With 100 fs pulses, Breton et al.<sup>35</sup> observed saturation of the 800 nm charge transfer bleach at  $2 \times 10^7\text{ photons}/\mu\text{m}^2$  upon excitation of B in reaction centers from *Rps. viridis*. Using 30 ps pulses at 870 nm to excite  $P_-$  in reaction centers from *Rb. sphaeroides*, Akhmanov et al.<sup>81</sup> observed that the charge separation quantum yield had dropped by a factor of 2 at  $10^8\text{ photons}/\mu\text{m}^2$ . The

experiments reported here were carried out at  $1.4 \times 10^6\text{ photons}/\mu\text{m}^2$ , which we estimate reduces the charge separation yield 6% by saturation. From the measurement of the number of absorbed photons, we calculate that 7% of the reaction centers are photoexcited. Since there are two accessory bacteriochlorophylls in each reaction center, one would expect roughly 7% of the excited reaction centers to be doubly excited. A doubly excited reaction center can produce only one charge separation, so the observed 6% reduction in charge transfer quantum yield is in accord with saturation by excitation of multiple pigments within a single reaction center.

It is also possible to saturate the optical transition on a single pigment. Since the laser pulse spectrum covers the entire B band, we approximate it as a single line and neglect dephasing during the pulse. We calculate saturation from the pulse area  $\theta = \int_{-\infty}^{+\infty} \vec{\mu} \cdot \vec{E}(t) dt/\hbar$ , where  $\vec{\mu}$  is the transition dipole vector and the vector  $\vec{E}(t)$  gives the electric field envelope.<sup>82</sup> From the  $Q_y$  transition dipole for bacteriochlorophyll *a* in diethyl ether<sup>83</sup> and acetone<sup>84</sup> ( $\mu = 6.3\text{ D}$ ) and the electric field envelope at the center of the beam  $E(t) = E_0 \exp(-t^2/2\tau^2)$ , where  $E_0 = 5.7 \times 10^7\text{ V/m}$  and  $\tau = 16\text{ fs}$  (22 fs fwhm pulse with 500 pJ energy), we calculate a pulse area  $\theta = 2\sqrt{2}\pi E_0 \tau \mu/\hbar = 0.93\text{ rad}$ , which corresponds to a  $\sin^2(\theta/2) = 0.20$  excitation probability for a transition dipole aligned parallel to the field. Averaging over all reaction center orientations yields an excitation probability of  $(1 - (\sin(\theta)/\theta))/2 \approx 0.069$ , in unreasonably good agreement with the observed 7% fraction of excited reaction centers. Comparing the calculated excitation probability to the unsaturated result  $1/3(\theta/2)^2 \approx 0.072$ , the excited state population would be reduced approximately 4% by saturation of individual bacteriochlorophyll pigments.

The initial anisotropy is  $r(0) = 0.404 (\pm 0.015)$  within experimental error equal to the value  $r(0) = 2/5$  expected for dipole excitation of a single pigment or incoherent excitation of several pigments. The power dependence of the anisotropy at the maximum pump–probe signal suggests that anisotropy values are reduced about 1% by saturation effects for the 500 pJ pulses used in the experiments. A similar reduction in the initial pump–probe anisotropy was observed for the dye IR144. In both reaction centers and IR144, a likely explanation for the anisotropy decrease with pump-power is preferential saturation of molecules with transition moments aligned parallel to the electric field of the optical pulse. For bacteriochlorophylls with transition dipoles aligned parallel to the field, the calculated excited state population is reduced about 7% ( $(\sin^2(\theta/2) - \sin^2(\theta/2))/(\theta/2)^2$ ) by saturation: this is larger than the angle averaged result of 4% saturation and will cause a decrease in the pump–probe anisotropy. We do not see any sign of the  $r(0) = 0.50$  initial anisotropy predicted for the accessory bacteriochlorophyll dimer on the basis of recent theoretical work.<sup>55–58</sup>

Under single excitation conditions and nonsaturating pulse intensities, an  $\sim 400\text{ fs}$  bleach decay component seen upon 800 nm excitation of the accessory bacteriochlorophylls in all previous studies<sup>35,36,45</sup> is not present. It is sobering to note that ref 35 reported the 400 fs decay amplitude varied linearly with pump pulse energy when the pump pulse energy was varied by a factor of 16 (from  $5 \times 10^6$  to  $8 \times 10^7\text{ photons}/\mu\text{m}^2$ ). Comparison with calculations is evidently necessary to establish that an experiment is actually being performed in the low intensity limit.

Fitting our data to a kinetic model favors a two-step energy transfer mechanism in which energy is transferred from B to the nearly isoenergetic state  $P_+$  of the special pair, which then internally converts to the lower exciton state  $P_-$ . The hypothesis that  $P_+$  is the initial acceptor is supported by the observation

of weak quantum beats (125 and 227  $\text{cm}^{-1}$  frequencies) with a near-zero anisotropy. The best fit energy transfer time constant of  $\sim 80$  fs is sufficiently abrupt to set vibrational wavepackets of these frequencies in motion on the upper exciton component of the special pair. The 125  $\text{cm}^{-1}$  frequency is consistent with excitation of a 128  $\text{cm}^{-1}$  vibration found only for the special pair and not for the accessory bacteriochlorophylls.<sup>41,74–79</sup> Evidently the energy transfer from B to  $\text{P}^+$  creates vibrational wavepackets on the special pair. The energy transfer process is completed by an  $\sim 140$  fs internal conversion between  $\text{P}_+$  and  $\text{P}_-$ . Over the first few hundred femtoseconds, the best single exponential fit to the rise of  $\text{P}_-$  population calculated from the kinetic model has a time constant of  $\sim 170$  fs. This time constant is in reasonable agreement with best fit  $\text{P}_-$  rise times of  $\sim 120$  fs measured after excitation of B with 100 fs pulses,<sup>38,40</sup> especially given the uncertainties in the kinetic model parameters and difficulties in measuring transient responses which are close to the pulse duration.

The above conclusions differ somewhat from those of Haran et al.,<sup>39</sup> who used 60 fs pulses to observe the bleach rise near 950 nm after excitation with 40–60 fs pulses centered at 810 nm. Haran et al. reported anisotropy values which were lower than expected for energy transfer from B to  $\text{P}_-$  and conclude from this that the states B and  $\text{P}_+$  are heavily mixed by excitonic interactions and that energy transfer takes place from this mixed B/ $\text{P}_+$  state to  $\text{P}_-$  in 120 fs. There are several experimental differences between the two studies: (1) the pulse durations used in this study are a factor of 2–3 shorter than those used in ref 39; (2) the fluence used in this study was about a factor of 4 lower than that used in ref 39; (3) the spectrum of the reaction centers used in this study (Figure 2) has less overlap between the peaks labeled P, B, and H than the spectrum in Figure 1 of ref 39. Excitonic coupling models predict that  $\text{P}_+$  contributes 20–30% of the intensity of the 800 nm band.<sup>21–25,63</sup> Overlap of the 30 nm fwhm pulses centered at 810 nm used in ref 39 with a Gaussian decomposition of the 800 nm band predicts excitation of 58% B, 33%  $\text{P}_+$ , 5%  $\text{P}_-$ , and 3% H. The anisotropies calculated for incoherent excitation of B (70%) and  $\text{P}_+$  (30%) using the model presented here *quantitatively* reproduce all the anisotropies in Table 3 of ref 39.<sup>85</sup>

The  $\sim 80$  fs B to  $\text{P}_+$  energy transfer is similar in time scale to a fast internal conversion between two electronic states of a single molecule. However, it differs from internal conversion because ground state absorption does not recover after internal conversion between two excited states within a single molecule. Energy transfer between pigments must transform continuously into internal conversion as the pigment–pigment coupling is increased.<sup>86</sup> Evidently, the ultrafast “energy transfer” in the reaction center lies between normal energy transfer and normal internal conversion and has some of the properties of each.

The hypothesis that energy transfer proceeds from B to  $\text{P}_+$  is consistent with Franck–Condon requirements for any rapid internal conversion process. All radiationless transitions depend on a Franck–Condon overlap factor between initial and final electronic states.<sup>10,11,14</sup> This factor can be estimated as

$$J = \frac{\int F(\nu) \epsilon(\nu) \nu^{-4} d\nu}{\int F(\nu) \nu^{-3} d\nu \int \epsilon(\nu) \nu^{-1} d\nu} \quad (10)$$

where  $F$  is the fluorescence quantum spectrum of the donor and  $\epsilon$  is the molar extinction coefficient of the acceptor as a function of frequency,  $\nu$ . Because the  $1/(80 \text{ fs})$  energy transfer rate is 2 orders of magnitude larger than the  $1/(2 \text{ ps})$  Förster dipole–dipole rate calculated for B  $\rightarrow$   $\text{P}_+$  energy transfer in the weak coupling limit,<sup>26</sup> a Golden rule analysis would lead to the conclusion that the electronic matrix element must be 1 order

of magnitude larger than the dipole–dipole coupling. This is inconsistent with the energy gap between B and  $\text{P}_+$ . Most probably, however, the energy transfer process is coherent and cannot be adequately described by a kinetic rate.<sup>70–72,76</sup> Assuming a B– $\text{P}_+$  Franck–Condon factor of unity,<sup>26</sup> the calculated dipole–dipole coupling matrix element between  $\text{B}_L$  and  $\text{P}_+$  (or  $\text{B}_M$  and  $\text{P}_+$ ) is  $V \approx 70 \text{ cm}^{-1}$ , nearly one-half the B to  $\text{P}_+$  energy gap. This suggests that the strong coupling limit of Förster theory,<sup>10</sup> which gives a “rate” of  $k \approx 4V/h \approx (1/(120 \text{ fs}))$  may be applicable. Energy is assumed to be coherently oscillating back and forth between chromophores in the strong coupling limit of Förster theory, so the strong-coupling energy transfer rate neglects damping (e.g.,  $\text{P}_+ \rightarrow \text{P}_-$  internal conversion) in the reaction center. The strong coupling “rate” does not describe an exponential process and thus has a somewhat arbitrary definition<sup>10</sup> but appears to be reasonably close to the observed energy transfer rate in that the population of B is calculated to decay by  $(1/e)$  in  $\approx 70$  fs. Because of the van der Waals contact between B and P, it may also be necessary to include short-range interactions such as orbital penetration and exchange in calculating the electronic coupling.<sup>13,17</sup> A complete treatment of energy transfer in the strong-coupling limit which includes electronic coherence, electronic dephasing, and their effect on the anisotropy is obviously desirable and seems to require refinements in the theory.

**Acknowledgment.** We would like to thank James R. Norris, Julia Popov, Maxim Popov, and S. N. Dikshit for the reaction center samples and helpful advice. This work was supported by the National Science Foundation. Y.N. thanks the JSPS for a postdoctoral fellowship for research abroad.

## References and Notes

- (1) Darnell, J.; Lodish, H.; Baltimore, D. *Molecular Cell Biology*, 2nd ed.; Scientific American Books: New York, 1990.
- (2) Clayton, R. K. *Photosynthesis: physical mechanisms and chemical patterns*; Cambridge University Press: New York, 1980.
- (3) Fleming, G. R.; van Grondelle, R. *Phys. Today* **1994** (February), 48–55.
- (4) Diesenhofer, J.; Epp, O.; Miki, K.; Huber, R.; Michel, H. *Nature* **1985**, *318*, 618–624.
- (5) Michel, H.; Diesenhofer, J. *Science* **1989**, *245*, 1463–1473.
- (6) Chang, C.-H.; El-Kabbani, O.; Tiede, D.; Norris, J.; Schiffer, M. *Biochemistry* **1991**, *30*, 5352–5360.
- (7) El-Kabbani, O.; Chang, C.-H.; Tiede, D.; Norris, J.; Schiffer, M. *Biochemistry* **1991**, *30*, 5361–5369.
- (8) Ermler, U.; Fritzsche, G.; Buchanan, S. K.; Michel, H. *Structure* **1994**, *2*, 925–936.
- (9) McDermott, G.; Prince, S. M.; Freer, A. A.; Hawthornwaite-Lawless, A. M.; Papiz, M. Z.; Cogdell, R. J.; Isaacs, N. W. *Nature* **1995**, *374*, 517–521.
- (10) Förster, T. Delocalized excitation and excitation transfer. In *Modern Quantum Chemistry*; Sinanoglu, O., Ed.; Academic Press, Inc.: New York, 1965; Vol. III, pp 93–137.
- (11) Dexter, D. L. *J. Chem. Phys.* **1953**, *21*, 834–850.
- (12) van Grondelle, R.; Dekker, J. P.; Gillbro, T.; Sundstrom, V. *Biochim. Biophys. Acta* **1994**, *1187*, 1–65.
- (13) Scholes, G. D.; Ghiggino, K. P. *J. Phys. Chem.* **1994**, *98*, 4580–4590.
- (14) Scholes, G. D.; Ghiggino, K. P. *J. Chem. Phys.* **1994**, *101*, 1251.
- (15) Scholes, G. D.; Ghiggino, K. P. *J. Photochem. Photobiol. A* **1994**, *80*, 355.
- (16) Scholes, G. D.; Ghiggino, K. P. *J. Chem. Phys.* **1995**, *103*, 8873.
- (17) Scholes, G. D.; Harcourt, R. D.; Ghiggino, K. P. *J. Chem. Phys.* **1995**, *102*, 9574.
- (18) Warshel, A.; Parson, W. W. *J. Am. Chem. Soc.* **1987**, *109*, 6152–6163.
- (19) Warshel, A.; Parson, W. W. *J. Am. Chem. Soc.* **1987**, *109*, 6143–6152.
- (20) Scherer, P. O. J.; Fischer, S. F. *J. Phys. Chem.* **1989**, *93*, 1633–1637.
- (21) Won, Y.; Friesner, R. A. *J. Phys. Chem.* **1988**, *92*, 2208–2214.
- (22) Won, Y.; Friesner, R. A. *J. Phys. Chem.* **1988**, *92*, 2214–2219.
- (23) Friesner, R. A.; Won, Y. *Biochim. Biophys. Acta* **1989**, *77*, 99–122.
- (24) Lathrop, E. J. P.; Friesner, R. A. *J. Phys. Chem.* **1994**, *98*, 3056–3066.

- (25) Scherer, P. O. J.; Fischer, S. F.; Lancaster, C. R. D.; Fritzsche, G.; Schmidt, S.; Arlt, T.; Dressler, K.; Zinth, W. *Chem. Phys. Lett.* **1994**, *223*, 110–115.
- (26) Jean, J. M.; Chan, C.-K.; Fleming, G. R. *Isr. J. Chem.* **1988**, *28*, 169–175.
- (27) Bixon, M.; Jortner, J.; Michel-Beyerle, M. E. *Biochim. Biophys. Acta* **1991**, *1056*, 301–315.
- (28) Marchi, M.; Gehlen, J. N.; Chandler, D.; Newton, M. J. *J. Am. Chem. Soc.* **1993**, *115*, 4178–4190.
- (29) Gehlen, J. N.; Marchi, M.; Chandler, D. *Science* **1994**, *263*, 499–502.
- (30) Egger, R.; Mak, C. H. *J. Phys. Chem.* **1994**, *98*, 9903–9918.
- (31) Schmidt, S.; Arlt, T.; Hamm, P.; Huber, H.; Nagele, T.; Wachtveitl, J.; Meyer, M.; Scheer, H.; Zinth, W. *Chem. Phys. Lett.* **1994**, *223*, 116–120.
- (32) Warshel, A.; Chu, Z. T.; Parson, W. W. *J. Photochem. Photobiol. A* **1994**, *82*, 123–128.
- (33) Warshel, A.; Parson, W. W. *Ann. Rev. Phys. Chem.* **1991**, *42*, 279–309.
- (34) Chang, J. C. *J. Chem. Phys.* **1977**, *67*, 3901.
- (35) Breton, J.; Martin, J.-L.; Migus, A.; Antonetti, A.; Orszag, A. *Proc. Natl. Acad. Sci. U.S.A.* **1986**, *83*, 5121–5125.
- (36) Breton, J.; Martin, J.-L.; Fleming, G. R.; Lambry, J.-C. *Biochemistry* **1988**, *27*, 8276–8284.
- (37) Walker, G. C.; Maiti, S.; Reid, G. D.; Wynne, K.; Moser, C. C.; Pippenger, R. S.; Cohen, B. R.; Dutton, P. L.; Hochstrasser, R. M. Femtosecond Infrared Spectroscopy of the Photosynthetic Reaction Center. In *Ultrafast Phenomena IX*; Mourou, G., Zewail, A. H., Barbara, P. F., Knox, W. H., Eds.; Springer-Verlag: New York, 1994; pp 439–440.
- (38) Wynne, K.; Haran, G.; Reid, G. D.; Moser, C. C.; Dutton, P. L.; Hochstrasser, R. M. *J. Phys. Chem.* **1996**, *100*, 5140–5148.
- (39) Haran, G.; Wynne, K.; Moser, C. C.; Dutton, P. L.; Hochstrasser, R. M. *J. Phys. Chem.* **1996**, *100*, 5562–5569.
- (40) Jonas, D. M.; Lang, M. J.; Nagasawa, Y.; Bradforth, S. E.; Dikshit, S. N.; Jimenez, R.; Joo, T.; Fleming, G. R. Ultrafast Energy Transfer within the Bacterial Photosynthetic Reaction Center. In *Reaction Centers of Photosynthetic Bacteria: Structure and Dynamics*; Michel Beyerle, M. E., Ed.; Springer-Verlag: New York, in press.
- (41) Stanley, R. J.; Boxer, S. G. *J. Phys. Chem.* **1995**, *99*, 859–863.
- (42) Wraight, C. A.; Clayton, R. K. *Biochim. Biophys. Acta* **1973**, *333*, 246–260.
- (43) Hartwich, G.; Friese, M.; Scheer, H.; Ogrodnick, A.; Michel-Beyerle, M. E. *Chem. Phys.* **1995**, *197*, 423–434.
- (44) Michel Beyerle, M. E. In *Reaction Centers of Photosynthetic Bacteria: Structure and Dynamics*; Michel Beyerle, M. E., Ed.; Springer-Verlag: New York, in press.
- (45) Jia, Y.; Jonas, D. M.; Joo, T.; Nagasawa, Y.; Lang, M. J.; Fleming, G. R. *J. Phys. Chem.* **1995**, *99*, 6263–6266.
- (46) Wraight, C. A. *Biochim. Biophys. Acta* **1979**, *548*, 309.
- (47) Asaki, M. T.; Huang, C. P.; Garvey, D.; Zhou, J.; Kapteyn, H. C.; Murnane, M. M. *Opt. Lett.* **1993**, *18*, 977.
- (48) Pshenichnikov, M. S.; de Boeij, W. P.; Wiersma, D. A. *Opt. Lett.* **1994**, *19*, 572–574.
- (49) Beddard, G. S.; Doust, T.; Porter, G. *Chem. Phys.* **1981**, *61*, 17–23.
- (50) Landau, L. D.; Lifschitz, E. M. *Fluid Mechanics*, 2nd ed.; Pergamon Press: New York, 1987.
- (51) Demtröder, W. *Laser Spectroscopy*, 2nd ed.; Springer-Verlag: New York, 1982.
- (52) Vos, M. H.; Lambry, J.-C.; Robles, S. J.; Youvan, D. C.; Breton, J.; Martin, J.-L. *Proc. Natl. Acad. Sci. U.S.A.* **1991**, *88*, 8885.
- (53) Du, M.; Rosenthal, S. J.; Xie, X.; DiMugno, T. J.; Schmidt, M.; Hanson, D. K.; Schiffer, M.; Norris, J. R.; Fleming, G. R. *Proc. Natl. Acad. Sci. U.S.A.* **1992**, *89*, 8517–8521.
- (54) Fleming, G. R. *Chemical Applications of Ultrafast Spectroscopy*; Oxford University Press: Oxford, U.K., 1985.
- (55) Knox, R. S.; Gülen, D. *Photochem. Photobiol.* **1992**, *57*, 40–43.
- (56) Wynne, K.; Hochstrasser, R. M. *Chem. Phys.* **1993**, *171*, 179–88.
- (57) Wynne, K.; Hochstrasser, R. M. *Chem. Phys.* **1993**, *173*, 539.
- (58) Wynne, K.; Hochstrasser, R. M. *J. Raman Spectrosc.* **1995**, *26*, 561–569.
- (59) Galli, C.; Wynne, K.; LeCours, S. M.; Therien, M. J.; Hochstrasser, R. M. *Chem. Phys. Lett.* **1993**, *206*, 493–499.
- (60) Wynne, K.; Granakaran, S.; Galli, C.; Zhu, F.; Hochstrasser, R. M. *J. Lumin.* **1994**, *60–61*, 735–738.
- (61) Jonas, D. M.; Bradforth, S. E.; Passino, S. A.; Fleming, G. R. *J. Phys. Chem.* **1995**, *99*, 2594–2608.
- (62) Jonas, D. M.; Fleming, G. R. Vibrationally Abrupt Pulses in Pump-Probe Spectroscopy. In *Ultrafast processes in Chemistry and Photobiology*; El-Sayed, M. A., Tanaka, I., Molin, Y. N., Eds.; Blackwell Scientific: London, 1995; pp 225–256.
- (63) Reddy, N. R. S.; Kolaczowski, S. V.; Small, G. J. *J. Phys. Chem.* **1993**, *97*, 6934–6940.
- (64) Thompson, M. A.; Zerner, M. C.; Fajer, J. *J. Phys. Chem.* **1991**, *95*, 5693–5700.
- (65) Vos, M. H.; Lambry, J.-C.; Robles, S. J.; Youvan, D. C.; Breton, J.; Martin, J.-L. *Proc. Natl. Acad. Sci. U.S.A.* **1992**, *89*, 613–617.
- (66) Joo, T.; Yiwei, J.; Yu, J.-Y.; Jonas, D. M.; Fleming, G. R. *J. Phys. Chem.* **1996**, *100*, 2399–2409.
- (67) Pullerits, T.; Chachisvilis, M.; Jones, M. R.; Hunter, C. N.; Sundström, V. *Chem. Phys. Lett.* **1994**, *224*, 355–365.
- (68) Hess, S.; Visscher, K. J.; Pullerits, T.; Sundström, V.; Fowler, G. J. S.; Hunter, C. N. *Biochem. J.* **1994**, *33*, 8300–8305.
- (69) Cross, A. J.; Fleming, G. R. *Biophys. J.* **1984**, *46*, 45.
- (70) Jean, J. M.; Friesner, R. A.; Fleming, G. R. *J. Chem. Phys.* **1992**, *96*, 5827–5842.
- (71) Jean, J. M. *J. Chem. Phys.* **1994**, *101*, 10464–10473.
- (72) Jean, J. M.; Fleming, G. R. *J. Chem. Phys.* **1995**, *103*, 2092–2101.
- (73) Reimers, J. R.; Hush, N. S. *J. Am. Chem. Soc.* **1995**, *117*, 1302–1308.
- (74) Vos, M. H.; Rappaport, F.; Lambry, J.-C.; Breton, J.; Martin, J.-L. *Nature* **1993**, *363*, 320–325.
- (75) Vos, M. H.; Jones, M. R.; Hunter, C. N.; Breton, J.; Martin, J.-L. *Proc. Natl. Acad. Sci. U.S.A.* **1994**, *91*, 12701–12705.
- (76) Vos, M. H.; Jones, M. R.; Hunter, C. N.; Breton, J.; Lambry, J.-C.; Martin, J.-L. *Biochemistry* **1994**, *33*, 6750–6757.
- (77) Shreve, A. P.; Cherepy, N. J.; Franzen, S.; Boxer, S. G.; Mathies, R. A. *Proc. Natl. Acad. Sci. U.S.A.* **1991**, *88*, 11207–11211.
- (78) Cherepy, N. R.; Schreve, A. P.; Moore, L. J.; Franzen, S.; Boxer, S. G.; Mathies, R. A. *J. Phys. Chem.* **1994**, *98*, 6023–6029.
- (79) Lyle, P. A.; Kolaczowski, S. V.; Small, G. J. *J. Phys. Chem.* **1993**, *97*, 6924–6933.
- (80) Scherer, N. F.; Jonas, D. M.; Fleming, G. R. *J. Chem. Phys.* **1993**, *99*, 153–168.
- (81) Akhmanov, S. A.; Borisov, A. Y.; Danielius, R. V.; Gadonas, R. A.; Kozlovskij, V. S.; Piskarskas, A. S.; Razjivin, A. P. Spectroscopy of Photoactive Centres by Tunable Picosecond Parametric Oscillators. In *Laser Spectroscopy IV*; Walther, H., Rothe, K. W., Eds.; Springer-Verlag: New York, 1979; pp 387–398.
- (82) Allen, L.; Eberly, J. H. *Optical Resonance and Two-Level Atoms*; Dover: Mineola, NY, 1987.
- (83) Shipman, L. L. *Photochem. Photobiol.* **1977**, *31*, 157–167.
- (84) Scherz, A.; Parson, W. W. *Biochim. Biophys. Acta* **1984**, *766*, 653–665.
- (85) This conclusion is based on the following state to state anisotropies: for 810 nm pump and 950 nm probe,  $r(B-P_-) = 0.25$  and  $r(P_+-P_-) = -0.20$ , yielding an effective anisotropy of  $r = 0.12$  (experiment  $r = 0.11 \pm 0.01$ ); for 810 nm pump and 1215 nm probe,  $r(B-P_L) = 0.22$  and  $r(P_+-P_L) = -0.12$ , yielding an effective anisotropy of  $r = 0.12$  (experiment  $r = 0.12 \pm 0.01$ ); for 810 nm pump and 3840 nm probe,  $r(B-CT) = 0.17$  and  $r(P_+-CT) = -0.20$ , yielding an effective anisotropy of  $r = 0.06$  (experiment  $r = 0.05 \pm 0.01$ ). Experimental anisotropies are taken from Table 3 of ref 39. The charge transfer transition dipole is assumed to point from Mg to Mg on the special pair. All effective anisotropies are calculated assuming that a 30 nm bandwidth pulse centered at 810 nm excites 70% B and 30% P<sub>+</sub>.
- (86) This is most easily seen by formally regarding the uncoupled molecules as a single supermolecule with a single ground state. The ground state absorption of unexcited pigments becomes an excited state absorption in the uncoupled (energy transfer) limit of the formally coupled system. See Figure 10.